QCD studies with e^+e^- annihilation data at 172-189 GeV

The OPAL Collaboration

G. Abbiendi[2], K. Ackerstaff[8], P.F. Akesson[3], G. Alexander[22], J. Allison[16], K.J. Anderson[9], S. Arcelli[17], S. Asai[23], S.F. Ashby[1], D. Axen[27], G. Azuelos[18,a], I. Bailey[26], A.H. Ball[8], E. Barberio[8], R.J. Barlow[16], J.R. Batley[5], S. Baumann[3], T. Behnke[25], K.W. Bell[20], G. Bella[22], A. Bellerive[9], S. Bentvelsen[8], S. Bethke[14,i], O. Biebel[14,i], A. Biguzzi[5], I.J. Bloodworth[1], P. Bock[11], J. Böhme[14,h], O. Boeriu[10], D. Bonacorsi[2], M. Boutemeur[31], S. Braibant[8], P. Bright-Thomas[1], L. Brigliadori[2], R.M. Brown[20], H.J. Burckhart[8], J. Cammin[3], P. Capiluppi[2], R.K. Carnegie[6], A.A. Carter[13], J.R. Carter[5], C.Y. Chang[17], D.G. Charlton[1,b], D. Chrisman[4], C. Ciocca[2], P.E.L. Clarke[15], E. Clay[15], I. Cohen[22], O.C. Cooke[8], J. Couchman[15], C. Couyoumtzelis[13], R.L. Coxe[9], M. Cuffiani[2], S. Dado[21], G.M. Dallavalle[2], S. Dallison[16], R. Davis[28], A. de Roeck[8], P. Dervan[15], K. Desch[25], B. Dienes[30,h], M.S. Dixit[7], M. Donkers[6], J. Dubbert[31], E. Duchovni[24], G. Duckeck[31], I.P. Duerdoth[16], P.G. Estabrooks[6], E. Etzion[22], F. Fabbri[2], A. Fanfani[2], M. Fanti[2], A.A. Faust[28], L. Feld[10], P. Ferrari[12], F. Fiedler[25], M. Fierro[2], I. Fleck[10], A. Frey[8], A. Fürtjes[8], D.I. Futyan[16], P. Gagnon[12], J.W. Gary[4], G. Gaycken[25], C. Geich-Gimbel[3], G. Giacomelli[2], P. Giacomelli[2], D.M. Gingrich[28,a], D. Glenzinski[9], J. Goldberg[21], W. Gorn[4], C. Grandi[2], K. Graham[26], E. Gross[24], J. Grunhaus[22], M. Gruwé[25], P.O. Günther[3], C. Hajdu[29], G.G. Hanson[12], M. Hansroul[8], M. Hapke[13], K. Harder[25], A. Harel[21], C.K. Hargrove[7], M. Harin-Dirac[4], A. Hauke[3], M. Hauschild[8], C.M. Hawkes[1], R. Hawkings[25], R.J. Hemingway[6], C. Hensel[25], G. Herten[10], R.D. Heuer[25], M.D. Hildreth[8], J.C. Hill[5], P.R. Hobson[25], A. Hocker[9], K. Hoffman[8], R.J. Homer[1], A.K. Honma[8], D. Horváth[29,c], K.R. Hossain[28], R. Howard[27], P. Hüntemeyer[25], P. Igo-Kemenes[11], D.C. Imrie[25], K. Ishii[23], F.R. Jacob[20], A. Jawahery[17], H. Jeremie[18], M. Jimack[1], C.R. Jones[5], P. Jovanovic[1], T.R. Junk[6], N. Kanaya[23], J. Kanzaki[23], G. Karapetian[18], D. Karlen[6], V. Kartvelishvili[16], K. Kawagoe[23], T. Kawamoto[23], P.I. Kayal[28], R.K. Keeler[26], R.G. Kellogg[17], B.W. Kennedy[20], D.H. Kim[19], K. Klein[11], A. Klier[24], T. Kobayashi[23], M. Kobel[3], T.P. Kokott[3], M. Kolrep[10], S. Komamiya[23], R.V. Kowalewski[26], T. Kress[4], P. Krieger[6], J. von Krogh[11], T. Kuhl[3], M. Kupper[24], P. Kyberd[13], G.D. Lafferty[16], H. Landsman[21], D. Lanske[14], I. Lawson[26], J.G. Layter[4], A. Leins[31], D. Lellouch[24], J. Letts[12], L. Levinson[24], R. Liebisch[11], J. Lillich[10], B. List[8], C. Littlewood[5], A.W. Lloyd[1], S.L. Lloyd[13], F.K. Loebinger[16], G.D. Long[26], M.J. Losty[7], J. Lu[27], J. Ludwig[10], A. Macchiolo[18], A. Macpherson[28], W. Mader[3], M. Mannelli[8], S. Marcellini[2], T.E. Marchant[16], A.J. Martin[13], J.P. Martin[18], G. Martinez[17], T. Mashimo[23], P. Mättig[24], W.J. McDonald[28], J. McKenna[27], T.J. McMahon[1], R.A. McPherson[26], F. Meijers[8], P. Mendez-Lorenzo[31], F.S. Merritt[9], H. Mes[7], I. Meyer[5], A. Michelini[2], S. Mihara[23], G. Mikenberg[24], D.J. Miller[15], W. Mohr[10], A. Montanari[2], T. Mori[23], K. Nagai[8], I. Nakamura[23], H.A. Neal[12,f], R. Nisius[8], S.W. O'Neale[1], F.G. Oakham[7], F. Odorici[2], H.O. Ogren[12], A. Okpara[11], M.J. Oreglia[9], S. Orito[23], G. Pásztor[29], J.R. Pater[16], G.N. Patrick[20], J. Patt[10], R. Perez-Ochoa[8], P. Pfeifenschneider[14], J.E. Pilcher[9], J. Pinfold[28], D.E. Plane[8], B. Poli[2], J. Polok[8], M. Przybycień[8,d], A. Quadt[8], C. Rembser[8], H. Rick[8], S.A. Robins[21], N. Rodning[28], J.M. Roney[26], S. Rosati[3], K. Roscoe[16], A.M. Rossi[2], Y. Rozen[21], K. Runge[10], O. Runolfsson[8], D.R. Rust[12], K. Sachs[10], T. Saeki[23], O. Sahr[31], W.M. Sang[25], E.K.G. Sarkisyan[22], C. Sbarra[26], A.D. Schaile[31], O. Schaile[31], P. Scharff-Hansen[8], S. Schmitt[11], A. Schöning[8], M. Schröder[8], M. Schumacher[25], C. Schwick[8], W.G. Scott[20], R. Seuster[14,h], T.G. Shears[8], B.C. Shen[4], C.H. Shepherd-Themistocleous[5], P. Sherwood[15], G.P. Siroli[2], A. Skuja[17], A.M. Smith[8], G.A. Snow[17], R. Sobie[26], S. Söldner-Rembold[10,e], S. Spagnolo[20], M. Sproston[20], A. Stahl[3], K. Stephens[16], K. Stoll[10], D. Strom[19], R. Ströhmer[31], B. Surrow[8], S.D. Talbot[1], S. Tarem[21], R.J. Taylor[15], R. Teuscher[9], M. Thiergen[10], J. Thomas[15], M.A. Thomson[8], E. Torrence[8], S. Towers[6], T. Trefzger[31], I. Trigger[8], Z. Trócsányi[30,g], E. Tsur[22], M.F. Turner-Watson[1], I. Ueda[23], R. Van Kooten[12], P. Vannerem[10], M. Verzocchi[8], H. Voss[3], D. Waller[6], C.P. Ward[5], D.R. Ward[5], P.M. Watkins[1], A.T. Watson[1], N.K. Watson[1], P.S. Wells[8], T. Wengler[8], N. Wermes[3], D. Wetterling[11], J.S. White[6], G.W. Wilson[16], J.A. Wilson[1], T.R. Wyatt[16], S. Yamashita[23], V. Zacek[18], D. Zer-Zion[8]

[1] School of Physics and Astronomy, University of Birmingham, Birmingham B15 2TT, UK
[2] Dipartimento di Fisica dell' Università di Bologna and INFN, 40126 Bologna, Italy
[3] Physikalisches Institut, Universität Bonn, 53115 Bonn, Germany
[4] Department of Physics, University of California, Riverside CA 92521, USA
[5] Cavendish Laboratory, Cambridge CB3 0HE, UK
[6] Ottawa-Carleton Institute for Physics, Department of Physics, Carleton University, Ottawa, Ontario K1S 5B6, Canada
[7] Centre for Research in Particle Physics, Carleton University, Ottawa, Ontario K1S 5B6, Canada
[8] CERN, European Organisation for Particle Physics, 1211 Geneva 23, Switzerland

[9] Enrico Fermi Institute and Department of Physics, University of Chicago, Chicago IL 60637, USA

[10] Fakultät für Physik, Albert Ludwigs Universität, 79104 Freiburg, Germany

[11] Physikalisches Institut, Universität Heidelberg, 69120 Heidelberg, Germany

[12] Indiana University, Department of Physics, Swain Hall West 117, Bloomington IN 47405, USA

[13] Queen Mary and Westfield College, University of London, London E1 4NS, UK

[14] Technische Hochschule Aachen, III Physikalisches Institut, Sommerfeldstrasse 26-28, 52056 Aachen, Germany

[15] University College London, London WC1E 6BT, UK

[16] Department of Physics, Schuster Laboratory, The University, Manchester M13 9PL, UK

[17] Department of Physics, University of Maryland, College Park, MD 20742, USA

[18] Laboratoire de Physique Nucléaire, Université de Montréal, Montréal, Quebec H3C 3J7, Canada

[19] University of Oregon, Department of Physics, Eugene OR 97403, USA

[20] CLRC Rutherford Appleton Laboratory, Chilton, Didcot, Oxfordshire OX11 0QX, UK

[21] Department of Physics, Technion-Israel Institute of Technology, Haifa 32000, Israel

[22] Department of Physics and Astronomy, Tel Aviv University, Tel Aviv 69978, Israel

[23] International Centre for Elementary Particle Physics and Department of Physics, University of Tokyo, Tokyo 113-0033, and Kobe University, Kobe 657-8501, Japan

[24] Particle Physics Department, Weizmann Institute of Science, Rehovot 76100, Israel

[25] Universität Hamburg/DESY, II Institut für Experimental Physik, Notkestrasse 85, 22607 Hamburg, Germany

[26] University of Victoria, Department of Physics, P O Box 3055, Victoria BC V8W 3P6, Canada

[27] University of British Columbia, Department of Physics, Vancouver BC V6T 1Z1, Canada

[28] University of Alberta, Department of Physics, Edmonton AB T6G 2J1, Canada

[29] Research Institute for Particle and Nuclear Physics, 1525 Budapest, P O Box 49, Hungary

[30] Institute of Nuclear Research, 4001 Debrecen, P O Box 51, Hungary

[31] Ludwigs-Maximilians-Universität München, Sektion Physik, Am Coulombwall 1, 85748 Garching, Germany

Abstract. We have studied hadronic events from e⁺e⁻ annihilation data at centre-of-mass energies of $\sqrt{s}$ =172, 183 and 189 GeV. The total integrated luminosity of the three samples, measured with the OPAL detector, corresponds to 250 pb⁻¹.

We present distributions of event shape variables, charged particle multiplicity and momentum, measured separately in the three data samples. From these we extract measurements of the strong coupling α_s, the mean charged particle multiplicity $\langle n_{\rm ch} \rangle$ and the peak position ξ_0 in the $\xi_p = \ln(1/x_p)$ distribution.

In general the data are described well by analytic QCD calculations and Monte Carlo models. Our measured values of α_s, $\langle n_{\rm ch} \rangle$ and ξ_0 are consistent with previous determinations at $\sqrt{s} = M_{\rm Z^0}$.

1 Introduction

We study the general features of hadronic decays in e⁺e⁻ → (Z⁰/γ)* → q$\bar{\rm q}$ reactions at the highest available centre-of-mass (c.m.) energies, as a continuation of our earlier publications at c.m. energies of $\sqrt{s} = 130-136$ GeV [1] and $\sqrt{s} = 161$ GeV [2].

In the last three years LEP produced e⁺e⁻ collisions at centre-of-mass energies of $\sqrt{s} \approx 172$, 183 and 189 GeV. The total integrated luminosity measured with the OPAL detector at these energies corresponds to approximately 250 pb⁻¹.

Previous studies using e⁺e⁻ annihilation data at c.m. energies up to $\sqrt{s} = 183$ GeV have shown that QCD based

models and calculations give a good description of the observed data [1–10]. Here we examine the overall consistency of QCD at yet higher c.m. energies, with improved statistical precision owing to the dramatic increase in integrated luminosity at c.m. energies above $\sqrt{s} = 161$ GeV.

We determine the strong coupling strength α_s at each of the three energies. The large data sample at 189 GeV, together with the fact that the hadronization corrections become smaller at higher c.m. energies, allows a precision comparable with that achieved at $\sqrt{s} = M_{\rm Z^0}$ using event shapes. We compare our results to those obtained at lower c.m. energies, notably at $\sqrt{s} = M_{\rm Z^0}$. We also determine the charged particle distributions and study the evolution with the c.m. energy of the mean charged particle multiplicity and the peak position ξ_0 in the $\xi_p = \ln(1/x_p)$ distribution. Jet-multiplicity related observables have been analyzed and used to determine α_s at these c.m. energies in a separate study of e⁺e⁻ annihilation data taken by the JADE and OPAL experiments at c.m. energies between 35 and 189 GeV [11].

The majority of hadronic events produced at c.m. energies above the Z⁰ resonance are 'radiative' events in which initial state photon radiation reduces the energy of the hadronic system to about $M_{\rm Z^0}$. An experimental

[a] and at TRIUMF, Vancouver, Canada V6T 2A3

[b] and Royal Society University Research Fellow

[c] and Institute of Nuclear Research, Debrecen, Hungary

[d] and University of Mining and Metallurgy, Cracow

[e] and Heisenberg Fellow

[f] now at Yale University, Dept of Physics, New Haven, USA

[g] and Department of Experimental Physics, Lajos Kossuth University, Debrecen, Hungary

[h] and MPI München

[i] now at MPI für Physik, 80805 München

separation between radiative and non-radiative events is therefore required. In addition, at energies above 160 GeV, W^+W^- production becomes kinematically possible and contributes a significant background to the $(Z^0/\gamma)^* \to q\bar{q}$ events. For $\sqrt{s} > 180$ GeV, Z^0Z^0 production must also be taken into account.

In this paper we use similar techniques to those of our previous analysis of e⁺e⁻ annihilation data at c.m. energies of 130–136 GeV [1] and 161 GeV [2]. In Sect. 2 we briefly describe the OPAL detector, in Sect. 3 we describe the samples of data and simulated events and in Sect. 4 we explain our selection requirements and analysis procedures. In Sect. 5 we then present the results in the form of event shape variables, determination of α_s, charged particle multiplicities and momentum spectra. Section 6 gives a summary and conclusion.

2 The OPAL detector

The OPAL detector operates at the LEP e⁺e⁻ collider at CERN. A detailed description can be found in [12]. The analysis presented here relies mainly on the measurements of momenta and directions of charged tracks in the tracking chambers and of energy deposited in the electromagnetic and hadronic calorimeters of the detector.

All tracking systems are located inside a solenoidal magnet which provides a uniform axial magnetic field of 0.435 T along the beam axis[1]. The magnet is surrounded by a lead glass electromagnetic calorimeter and a hadron calorimeter of the sampling type. Outside the hadron calorimeter, the detector is surrounded by a system of muon chambers. There are similar layers of detectors in the forward and backward endcaps.

The main tracking detector is the central jet chamber. This device is approximately 4 m long and has an outer radius of about 1.85 m. It has 24 sectors with radial planes of 159 sense wires spaced by 1 cm. The momenta p of tracks in the x-y plane are measured with a precision $\sigma_p/p = \sqrt{0.02^2 + (0.0015 \cdot p[\text{GeV}/c])^2}$.

The electromagnetic calorimeters in the barrel and the endcap sections of the detector consist of 11704 lead glass blocks with a depth of 24.6 radiation lengths in the barrel and more than 22 radiation lengths in the endcaps.

3 Data and Monte Carlo samples

The three data samples at $\sqrt{s} \approx 172$, 183 and 189 GeV that are used in this analysis were recorded as part of the LEP-2 programme between 1996 and 1998. The luminosities, evaluated using small angle Bhabha collisions, and the mean c.m. energies are tabulated in Table 1.

Monte Carlo event samples were generated at c.m. energies of 172.0, 183.0 and 189.0 GeV, including a full simulation of the OPAL detector [13]. Events for the process e⁺e⁻ $\to (Z^0/\gamma)^* \to q\bar{q}$, referred to as "$(Z^0/\gamma)^*$ events", were generated using the PYTHIA 5.722 [14] parton shower Monte Carlo code with initial and final state photon radiation and fragmentation of the parton final state handled by the routines of JETSET 7.408 [14]. The simulation parameters have been tuned to OPAL data taken at the Z^0 peak [15]. The JETSET Monte Carlo is able to provide a good description of experimental data for e⁺e⁻ annihilations with c.m. energies from 10 GeV to 161 GeV [1,3–6, 10].

As an alternative fragmentation model, we generated events with the HERWIG 5.9 [16] parton shower Monte Carlo program, also tuned to OPAL data, as described in [2,15]. As an alternative model for initial state radiation (ISR) the YFS3ff 3.6 [17] generator was used, coupled to the same JETSET routines to handle the parton final states.

In addition we generated events of the type e⁺e⁻ $\to 4$ fermions (diagrams without intermediate gluons). These 4-fermion events, in particular those with four quarks in the final state, constitute a major background for this analysis. Simulated 4-fermion events with quarks and leptonic final states were generated using the GRC4F 1.2 Monte Carlo Model [18]. The final states were produced via s-channel or t-channel diagrams and include W^+W^- events. This generator is interfaced to JETSET 7.4 using the same parameter-set for the parton shower, fragmentation and decays as for $(Z^0/\gamma)^*$ events.

Two other possible sources of background events were simulated. Hadronic two-photon processes were evaluated using PYTHIA, HERWIG and PHOJET [19]. Production of e⁺e⁻ $\to (Z^0/\gamma)^* \to \tau\bar{\tau}$ was evaluated using KORALZ [20].

In addition to the Monte Carlo event generators discussed above, we use the event generators ARIADNE 4.08 [21] and COJETS 6.23 [22]. ARIADNE is used to provide a systematic check on the hadronization corrections for our α_s measurement (Sect. 5.2). In contrast to the other models, COJETS is based on a parton shower model using independent fragmentation and does not take coherence effects into account. Both COJETS and ARIADNE are used in addition to PYTHIA and HERWIG to compare to our corrected data distributions. The parameter sets used for ARIADNE and COJETS are documented in [21] and [23]; both models provide a good description of global e⁺e⁻ event properties at $\sqrt{s} = M_{Z^0}$, as do PYTHIA and HERWIG.

4 Analysis method

4.1 Selection of events

Hadronic events are identified using criteria as described in [24]. The efficiency of selecting non-radiative hadronic events is essentially unchanged with respect to lower c.m.

---

[1] In the OPAL coordinate system the x axis points towards the centre of the LEP ring, the y axis points upwards and the z axis points in the direction of the electron beam. The polar angle θ and the azimuthal angle ϕ are defined w.r.t. z and x, respectively, while r is the distance from the z-axis.

Table 1. Data samples at 172, 183 and 189 GeV. The luminosity and luminosity weighted mean c.m. energies are given in the first two rows. The rows labelled as 'ISR-fit selection' and 'Final selection' correspond to the number of events passing these criteria

		172 GeV	183 GeV	189 GeV
$\langle$c.m. energy$\rangle$	(GeV)	172.1	182.7	188.7
Luminosity	(pb^{-1})	10.4	57.2	186.3
Preselection		1318	6142	18954
'ISR-fit' Selection		**273**	**1447**	**4457**
4-fermion background	%	20.3	26.6	29.4
Efficiency non-rad events	%	82.6	83.3	82.9
Final selection		**228**	**1098**	**3277**
4-fermion background	%	7.3	9.0	10.1
Efficiency non-rad events	%	79.4	79.4	78.5

energies and is approximately 98%[25]. We define as particles tracks recorded in the tracking chambers and clusters recorded in the electromagnetic calorimeter. The tracks are required to have transverse momentum to the beam axis $p_T > 150$ MeV/c, a number of hits in the jet chamber $N_{hits} \geq 40$, a distance of the point of closest approach to the collision point in the $r - \phi$ plane $d_0 \leq 2$ cm and in the z direction $z_0 \leq 25$ cm. The clusters in the electromagnetic calorimeter are required to have a minimum energy of 100 MeV in the barrel and 250 MeV in the endcap sections [1].

To reject background from e⁺e⁻ $\rightarrow \tau^+\tau^-$ and $\gamma\gamma \rightarrow$ q$\bar{\text{q}}$ events and to ensure the events are well contained in the OPAL detector we require at least seven accepted tracks, and the cosine of the polar angle of the thrust axis $|\cos\theta_T| < 0.9$. The number of events after this preselection, for each c.m. energy, are listed in Table 1.

To reject radiative events, we determine the effective c.m. energy $\sqrt{s'}$ of the observed hadronic system as follows [26]. Isolated photons in the electromagnetic calorimeter are identified, and the remaining particles are formed into jets using the Durham [27] algorithm with a value for the resolution parameter $y_{\text{cut}} = 0.02$. The energy of additional photons emitted close to the beam directions is estimated by performing three separate kinematic fits assuming zero, one or two such photons. The probabilities of the fits are used to select the most likely of these three. The value of $\sqrt{s'}$ is then computed from the fitted momenta of the jets, excluding photons identified in the detector or close to the beam directions. The value of $\sqrt{s'}$ is set to $\sqrt{s}$ if the fit assuming zero initial state photons was selected. The 4-momenta of the measured particles are then boosted into the rest frame of the observed hadronic system.

To reject events with large initial-state radiation (ISR), we require $\sqrt{s} - \sqrt{s'} < 10$ GeV. This is referred to as the 'ISR-fit' selection. In Fig. 1a we compare the $\sqrt{s'}$ distribution of the data to simulated $(\text{Z}^0/\gamma)^*$ and 4-fermion events. The simulated $(\text{Z}^0/\gamma)^*$ events are classified into
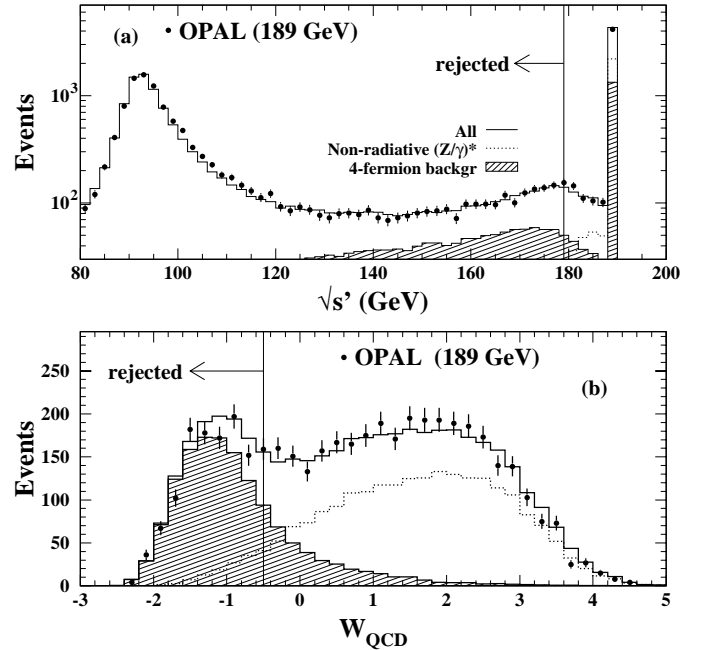

Fig. 1. a Distribution of reconstructed $\sqrt{s'}$ for the data (full points) with statistical errors. The PYTHIA predictions for all $(\text{Z}^0/\gamma)^*$ events (solid line) and for the non-radiative events, $\sqrt{s} - \sqrt{s'_{\text{true}}} < 1$ GeV, (dotted line) are also shown. The hatched area indicates the 4-fermion background predicted by the GRC4F Monte Carlo.
b Distribution of the QCD event weight W_{QCD}. The notation is identical to that of **a**

radiative events with $\sqrt{s} - \sqrt{s'_{\text{true}}} > 1$ GeV (where $\sqrt{s'_{\text{true}}}$ is the true effective c.m. energy, determined from Monte Carlo information), and non-radiative events, which is the complement. While about 27% of the selected $(\text{Z}^0/\gamma)^*$ events are by this definition radiative events, the fraction of events with $\sqrt{s} - \sqrt{s'_{\text{true}}} > 10$ GeV is only 5%. The contributions of 4-fermion events, simulated with GRC4F,

are indicated separately. The background from 4-fermion events and the efficiency of selecting non-radiative events are given in Table 1.

The background from e$^+$e$^-$ $\to \tau^+\tau^-$ and two-photon events of the type $\gamma\gamma \to$ q$\bar{\text{q}}$ is estimated from Monte Carlo samples to be less than 0.3% and is neglected.

In order to reduce the background of 4-fermion events on the remaining sample, we test the compatibility of the events with QCD-like production processes. A QCD event weight W_{QCD} is computed as follows. We force each event into a four-jet configuration in the Durham jet scheme and use the EVENT2 [28] program to calculate the $\mathcal{O}(\alpha_s^2)$ matrix element $|\mathcal{M}(p_1, p_2, p_3, p_4)|^2$ for the processes e$^+$e$^-$ $\to$ q$\bar{\text{q}}$q$\bar{\text{q}}$, q$\bar{\text{q}}$gg [29]. Since neither quark nor gluon identification is performed on the jets, we calculate the matrix element for each permutation of the jet-momenta and use the permutation with the largest value for the matrix element to define the event weight:

$$W_{\text{QCD}} = \max_{\{p_1, p_2, p_3, p_4\}} \log\left(|\mathcal{M}(p_1, p_2, p_3, p_4)|^2\right) \quad (1)$$

with p_i the momenta of reconstructed jets. Note that the definition of the event weight W_{QCD} contains kinematic information only and is independent of the value of α_s.

This weight W_{QCD} is expected to have large values for processes described by the QCD matrix element, originating from $(\text{Z}^0/\gamma)^* \to$ q$\bar{\text{q}}$, and smaller values for W$^+$W$^-$ events. In Fig. 1b we compare the data distribution of W_{QCD} to the expectations of our simulation. A clear separation between the $(\text{Z}^0/\gamma)^*$ and 4-fermion events is achieved by requiring $W_{\text{QCD}} \geq -0.5$. This requirement reduces the 4-fermion background considerably, as can be seen in Table 1, whereas the efficiency for selecting non-radiative $(\text{Z}^0/\gamma)^*$ events is only slightly reduced. In Fig. 2 we show, as an example, the effect of the 4-fermion background rejection on the distribution of thrust T, as defined in Sect. 5.1. The background from hadronic decays of W$^+$W$^-$ events has predominantly low values for T, and is largely removed by our selection.

4.2 Correction procedure

The remaining 4-fermion background in each bin has been estimated by Monte Carlo simulation and is subtracted from the observed bin content. A bin-by-bin multiplication procedure is used to correct the observed distributions for the effects of detector resolution and acceptance as well as for the presence of remaining radiative $(\text{Z}^0/\gamma)^*$ events. For the multiplicity measurement presented in Sect. 5.3, we use a matrix correction procedure to account for detector effects rather than a bin-by-bin procedure.

For the bin-by-bin correction procedure, each bin of each observable is corrected from the "detector level" to the "hadron level" using two samples of Monte Carlo $(\text{Z}^0/\gamma)^*$ events at each c.m. energy. The hadron level does not include initial state radiation or detector effects and allows all particles with lifetimes shorter than 3×10^{-10} s to decay. The detector level includes full simulation of the

OPAL detector and initial state radiation and contains only those events which pass the same cuts as are applied to the data. The bin-by-bin correction factors are derived from the ratio of the distributions at the hadron level to those at the detector level.

A bin-by-bin correction procedure is suitable for most quantities as the binsize is chosen to ensure the effects of finite resolution and acceptance do not cause significant migration (and therefore correlation) between bins. For the multiplicity measurement however, such a method is not readily applicable, due to the large correlations between bins.

The four-momenta of tracks and of the electromagnetic calorimeter clusters not associated with tracks were used to calculate event shapes. When a calorimeter cluster had associated tracks, their expected energy deposition was used to reduce double counting by correcting the cluster energy. If the energy of a cluster was smaller than the expected energy response of the associated tracks, the cluster energy was not used. The masses of all charged particles were set to the pion mass and the invariant masses of the energy clusters were assumed to be zero.

4.3 Systematic uncertainties

The experimental systematic uncertainty is estimated by repeating the analysis with varied experimental conditions. In order to reduce bin-to-bin fluctuations in the magnitudes of the systematic uncertainties we average the relative uncertainty over three neighbouring bins.

To allow for any inconsistencies caused by differences between the responses of the tracking or the calorimeter, three differences are formed for the quantities in each bin; between the standard result, the one obtained using tracks and all clusters and the one obtained using only tracks. The largest of them is taken as the systematic error.

The inhomogeneity of the response of the detector in the endcap region was allowed for by restricting the analysis to the barrel region of the detector, requiring the thrust axis of accepted events to lie within the range $|\cos\theta_T| < 0.7$. The event sample is reduced in size by approximately 27%. The corresponding systematic error is the deviation of the results from those of the standard analysis.

For observables measured using information from charged particles only, we evaluate an additional uncertainty on the track modelling. The maximum allowed distance of the point of closest approach of a track to the collision point in the r-ϕ plane d_0 was changed from 2 to 5 cm, the maximal distance in the z direction z_0 from 25 to 10 cm and the minimal number of hits from 40 to 80. These modifications change the number of tracks by up to approximately 12%. The quadratic sum of the deviations from the standard result is taken to be the systematic error due to the uncertainty of the track modelling.

Uncertainties arising from the selection of non-radiative events are estimated by repeating the analysis using a different technique[2] to determine the value for $\sqrt{s'}$. This technique differs from our standard $\sqrt{s'}$ algorithm in that in this case the kinematic fit assumes always one unob-
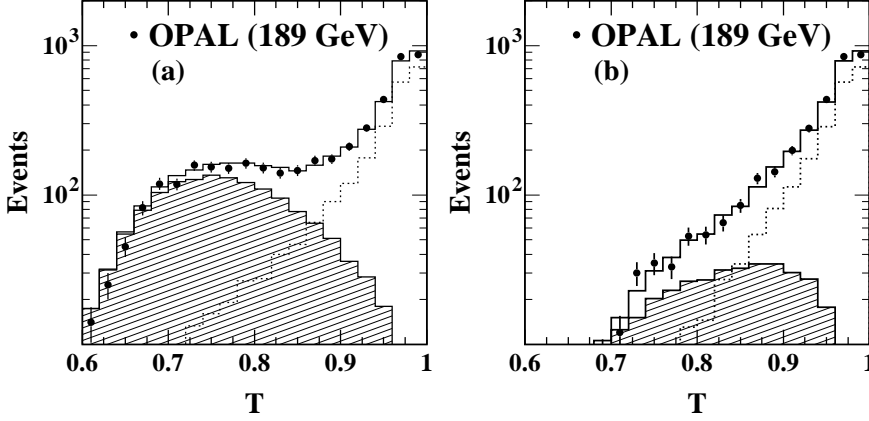
Fig. 2a,b. The effect of the W_{QCD} selection cut on the thrust distribution (see Fig. 1 for notation). In **a** the thrust distribution, on detector level, is shown before the W_{QCD} selection is applied. In **b** the same, after the selection on W_{QCD} is applied

served photon close to the beam direction for each event. The final event sample with this $\sqrt{s'}$ algorithm has an overlap of approximately 94% with the standard sample, and is reduced in size by 3%. The difference relative to the standard result is taken as the systematic error.

We evaluated our $(Z^0/\gamma)^*$ selection efficiencies using events generated with YFS3ff, which contains QED exponentiated matrix elements for ISR up to $O(\alpha_{EM}^3)$. Similar estimates of efficiencies are obtained if this model is used instead of PYTHIA, and therefore no additional systematic uncertainty is assigned.

Systematic uncertainties associated with the subtraction of the 4-fermion background events are estimated by varying the position of the cut-value on the QCD event weight W_{QCD} (see Fig. 1b). We vary this position to $W_{\mathrm{QCD}} \geq -0.8$ which increases the event sample by approximately 7%, and $W_{\mathrm{QCD}} \geq 0$ which decreases the event sample by approximately 12%. We take the maximum deviation from our standard result $W_{\mathrm{QCD}} \geq -0.5$ as the systematic uncertainty.

In addition we vary the predicted background to be subtracted, within its measured uncertainty of 5%[30], and use the largest difference from the standard result as a systematic uncertainty.

The difference in the results when we use simulated $(Z^0/\gamma)^*$ events generated using HERWIG instead of PYTHIA is taken as the uncertainty in the modelling of the $(Z^0/\gamma)^*$ events.

Note that due to the relativy small number of selected non-radiative events especially at $\sqrt{s} = 172$ GeV (see Table 1), part of the observed differences when the systematic conditions are varied may be due to statistical fluctuations. This is reflected in generally larger values for the systematic uncertainty of the results at $\sqrt{s} = 172$ GeV compared to those at the other c.m. energies.

5 Results

5.1 Event shapes

The properties of hadronic events may be characterised by a set of event shape observables. The following quantities are considered:

Thrust $\boldsymbol{T}$: defined by the expression[31,32]

$$T = \max_{\mathbf{n}} \left(\frac{\sum_i |p_i \cdot \mathbf{n}|}{\sum_i |p_i|} \right) \quad . \qquad (2)$$

The thrust axis $\mathbf{n}_T$ is the direction $\mathbf{n}$ which maximises the expression in parenthesis. A plane through the origin and perpendicular to $\mathbf{n}_T$ divides the event into two hemispheres H_1 and H_2.

Thrust major $\boldsymbol{T_{\mathbf{major}}}$. The maximisation in equation 2 is performed with the condition that $\mathbf{n}$ must lie in the plane perpendicular to $\mathbf{n}_T$. The resulting vector is called $\mathbf{n}_{T_{\mathrm{major}}}$.

Thrust minor $\boldsymbol{T_{\mathbf{minor}}}$. The expression in parenthesis is evaluated for the vector $\mathbf{n}_{T_{\mathrm{minor}}}$ which is perpendicular both to $\mathbf{n}_T$ and to $\mathbf{n}_{T_{\mathrm{major}}}$.

Oblateness $\boldsymbol{O}$. This observable is defined by $O = T_{\mathrm{major}} - T_{\mathrm{minor}}$ [33].

Sphericity $\boldsymbol{S}$ and Aplanarity $\boldsymbol{A}$. These observables are based on the momentum tensor

$$S^{\alpha\beta} = \frac{\sum_i p_i^\alpha p_i^\beta}{\sum_i p_i^2} \quad , \quad \alpha, \beta = 1, 2, 3 \quad .$$

The three eigenvalues Q_j of $S^{\alpha\beta}$ are ordered such that $Q_1 < Q_2 < Q_3$. These then define S [34,35] and A [36] by

$$S = \frac{3}{2}(Q_1 + Q_2) \quad \text{and} \quad A = \frac{3}{2}Q_1 \quad .$$

C-parameter. The momentum tensor $S^{\alpha\beta}$ is linearised to become

$$\Theta^{\alpha\beta} = \frac{\sum_i (p_i^\alpha p_i^\beta)/|p_i|}{\sum_i |p_i|} \quad , \quad \alpha, \beta = 1, 2, 3 \quad .$$

The three eigenvalues λ_j of this tensor define C[37] with

$$C = 3(\lambda_1\lambda_2 + \lambda_2\lambda_3 + \lambda_3\lambda_1) \quad .$$

Heavy Jet Mass $\boldsymbol{M_H}$. The hemisphere invariant masses are calculated using the particles in the two hemispheres H_1 and H_2. We define M_H [38,39] as the heavier mass, divided by $\sqrt{s}$.
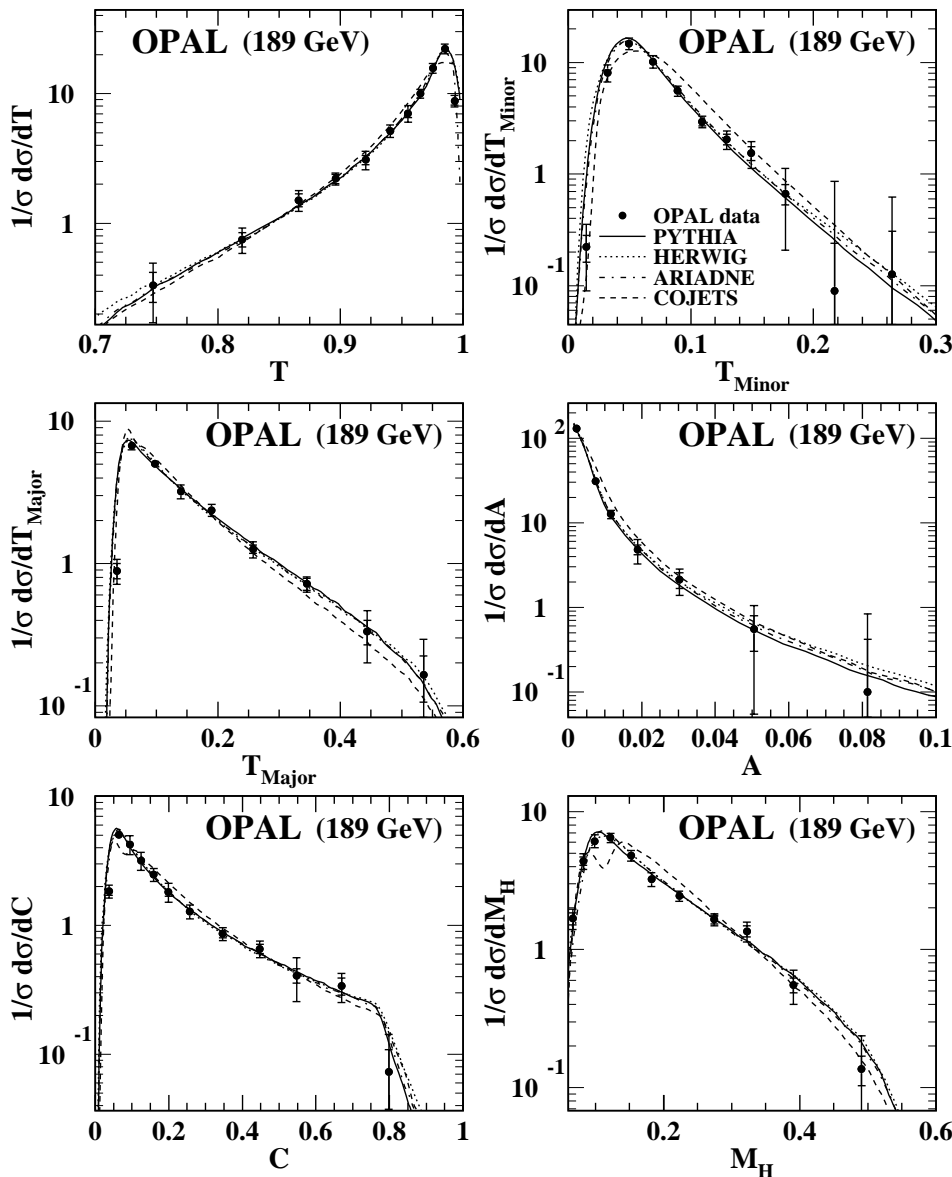
Fig. 3. Distributions at $\sqrt{s}$ = 189 GeV of the event shape observables thrust T, thrust major T_{major}, thrust minor T_{minor}, aplanarity A, C-parameter C and heavy jet mass M_H. Experimental statistical errors are delimited by the inner small horizontal bars. The total errors are shown by the outer horizontal error bars. Hadron level predictions from PYTHIA, HERWIG, ARIADNE and COJETS are also shown. Note that the deviation between data and COJETS at $M_H \approx 0.1$ could be observed already in our publication of the results at $\sqrt{s} = 161$ GeV [2]

Jet Broadening variables $\boldsymbol{B_T}$ and $\boldsymbol{B_W}$. These are defined by computing the quantity

$$B_k = \left(\frac{\sum_{i \in H_k} |p_i \times \mathbf{n}_T|}{2 \sum_i |p_i|} \right)$$

for each of the two event hemispheres, H_k, defined above. The two observables [40] are defined by

$$B_T = B_1 + B_2 \quad \text{and} \quad B_W = \max(B_1, B_2)$$

where B_T is the total and B_W is the wide jet broadening.

Transition value between 2 and 3 jets $\boldsymbol{y_{23}^D}$. The value of y_{cut} for the Durham jet scheme at which the event makes a transition between a 2-jet and a 3-jet assignment.

In the following, we use the symbol y to denote a generic event shape observable, where larger values of y indicate regions dominated by the radiation of hard gluons and small values of y indicate the region influenced by multiple soft gluon radiation. Note that thrust T forms an exception to this rule, as the value of T reaches one for events consisting of two collimated, back-to-back, jets. We therefore occasionally use $1 - T$ instead.

Figures 3 and 4 show the distributions of the event shape observables T, T_{major}, T_{minor}, A, C, M_H, S, O, B_T, B_W, and y_{23}^D, corrected for detector acceptance and initial state radiation, plotted at the weighted centres of the bins. The data obtained at 189 GeV are shown with the statistical and systematic uncertainties added in quadrature. The numerical values for all the event shape distributions, for c.m. energies of 172, 183 and 189 GeV, are listed in Tables 2 to 4.

With the statistics available at 189 GeV, all event shapes are determined with high precision. There are no significant deviations from the predictions of PYTHIA,

Table 2. Results $R(y) = 1/\sigma \cdot \mathrm{d}\sigma/\mathrm{d}y$ at $\sqrt{s} = 172$, 183 and 189 GeV for the event shape observables y: thrust T, thrust major T_{major}, thrust minor T_{minor} and aplanarity A. The first error is statistical, the second systematic

T	$R(T)$ (172 GeV)	$R(T)$ (183 GeV)	$R(T)$ (189 GeV)
0.700-0.780	$0.62 \pm 0.27 \pm 0.31$	$0.29 \pm 0.11 \pm 0.17$	$0.36 \pm 0.09 \pm 0.14$
0.780-0.850	$0.60 \pm 0.28 \pm 0.22$	$0.75 \pm 0.15 \pm 0.16$	$0.78 \pm 0.09 \pm 0.14$
0.850-0.880	$0.73 \pm 0.45 \pm 0.54$	$1.45 \pm 0.28 \pm 0.44$	$1.53 \pm 0.17 \pm 0.22$
0.880-0.910	$1.35 \pm 0.52 \pm 1.77$	$1.62 \pm 0.27 \pm 0.68$	$2.22 \pm 0.18 \pm 0.16$
0.910-0.930	$3.01 \pm 0.91 \pm 2.91$	$3.30 \pm 0.44 \pm 0.60$	$3.09 \pm 0.25 \pm 0.45$
0.930-0.950	$6.60 \pm 1.25 \pm 1.77$	$5.27 \pm 0.54 \pm 0.64$	$5.14 \pm 0.31 \pm 0.46$
0.950-0.960	$4.47 \pm 1.43 \pm 3.20$	$8.20 \pm 0.95 \pm 0.95$	$7.02 \pm 0.50 \pm 0.88$
0.960-0.970	$7.85 \pm 1.90 \pm 3.19$	$10.0 \pm 1.0 \pm 1.4$	$9.94 \pm 0.59 \pm 0.56$
0.970-0.980	$18.5 \pm 2.9 \pm 6.8$	$15.1 \pm 1.3 \pm 0.8$	$15.6 \pm 0.7 \pm 1.2$
0.980-0.990	$22.3 \pm 3.4 \pm 3.7$	$22.9 \pm 1.7 \pm 1.6$	$22.0 \pm 0.9 \pm 1.6$
0.990-1.000	$11.6 \pm 2.6 \pm 3.8$	$9.08 \pm 1.07 \pm 1.46$	$8.73 \pm 0.60 \pm 0.63$

T_{major}	$R(T_{\mathrm{major}})$ (172 GeV)	$R(T_{\mathrm{major}})$ (183 GeV)	$R(T_{\mathrm{major}})$ (189 GeV)
0.000-0.040	$1.68 \pm 0.57 \pm 0.62$	$0.92 \pm 0.19 \pm 0.16$	$0.88 \pm 0.11 \pm 0.14$
0.040-0.080	$7.33 \pm 0.99 \pm 0.68$	$7.17 \pm 0.47 \pm 0.34$	$6.66 \pm 0.26 \pm 0.35$
0.080-0.120	$4.87 \pm 0.72 \pm 0.18$	$4.96 \pm 0.36 \pm 0.27$	$5.00 \pm 0.21 \pm 0.22$
0.120-0.160	$3.23 \pm 0.60 \pm 1.09$	$3.22 \pm 0.29 \pm 0.60$	$3.19 \pm 0.17 \pm 0.33$
0.160-0.220	$2.03 \pm 0.40 \pm 0.28$	$2.32 \pm 0.20 \pm 0.19$	$2.36 \pm 0.12 \pm 0.20$
0.220-0.300	$1.07 \pm 0.27 \pm 0.38$	$1.18 \pm 0.14 \pm 0.24$	$1.26 \pm 0.08 \pm 0.14$
0.300-0.400	$0.49 \pm 0.21 \pm 0.21$	$0.84 \pm 0.12 \pm 0.21$	$0.73 \pm 0.07 \pm 0.05$
0.400-0.500	$0.29 \pm 0.18 \pm 0.13$	$0.23 \pm 0.08 \pm 0.12$	$0.35 \pm 0.06 \pm 0.12$
0.500-0.600	$0.33 \pm 0.17 \pm 0.24$	$0.033 \pm 0.075 \pm 0.124$	$0.18 \pm 0.06 \pm 0.11$

T_{minor}	$R(T_{\mathrm{minor}})$ (172 GeV)	$R(T_{\mathrm{minor}})$ (183 GeV)	$R(T_{\mathrm{minor}})$ (189 GeV)
0.000-0.020	$0.59 \pm 0.43 \pm 0.54$	$0.087 \pm 0.067 \pm 0.129$	$0.22 \pm 0.06 \pm 0.12$
0.020-0.040	$10.6 \pm 1.8 \pm 1.5$	$9.49 \pm 0.80 \pm 0.82$	$8.03 \pm 0.41 \pm 1.38$
0.040-0.060	$16.8 \pm 2.1 \pm 5.6$	$15.7 \pm 1.0 \pm 1.5$	$14.7 \pm 0.5 \pm 1.7$
0.060-0.080	$7.73 \pm 1.31 \pm 2.77$	$10.6 \pm 0.8 \pm 1.8$	$10.1 \pm 0.4 \pm 1.3$
0.080-0.100	$6.24 \pm 1.16 \pm 2.16$	$5.86 \pm 0.55 \pm 1.26$	$5.54 \pm 0.31 \pm 0.50$
0.100-0.120	$4.07 \pm 0.99 \pm 2.07$	$3.46 \pm 0.44 \pm 0.72$	$2.95 \pm 0.24 \pm 0.24$
0.120-0.140	$1.52 \pm 0.66 \pm 1.45$	$2.69 \pm 0.44 \pm 0.86$	$2.06 \pm 0.22 \pm 0.32$
0.140-0.160	$1.16 \pm 0.67 \pm 0.97$	$1.24 \pm 0.33 \pm 0.26$	$1.55 \pm 0.21 \pm 0.36$
0.160-0.200	$0.48 \pm 0.39 \pm 0.77$	$0.69 \pm 0.23 \pm 0.66$	$0.69 \pm 0.14 \pm 0.44$
0.200-0.240	$0.16 \pm 0.32 \pm 0.76$	$0.20 \pm 0.22 \pm 0.55$	$0.12 \pm 0.15 \pm 0.75$
0.240-0.300	$0.30 \pm 0.48 \pm 0.86$	$-.475 \pm 0.617 \pm 1.540$	$0.15 \pm 0.18 \pm 0.46$

A	$R(A)$ (172 GeV)	$R(A)$ (183 GeV)	$R(A)$ (189 GeV)
0.000-0.005	$119. \pm 10. \pm 34.$	$131. \pm 5. \pm 5.$	$129. \pm 3. \pm 9.$
0.005-0.010	$33.2 \pm 5.9 \pm 9.8$	$34.2 \pm 3.1 \pm 3.3$	$30.9 \pm 1.7 \pm 1.8$
0.010-0.015	$14.2 \pm 4.0 \pm 9.4$	$12.6 \pm 2.0 \pm 4.4$	$12.7 \pm 1.2 \pm 0.8$
0.015-0.025	$5.88 \pm 2.15 \pm 2.02$	$5.56 \pm 1.07 \pm 2.28$	$4.87 \pm 0.62 \pm 1.40$
0.025-0.040	$0.80 \pm 0.91 \pm 1.42$	$2.55 \pm 0.72 \pm 1.26$	$2.17 \pm 0.44 \pm 0.58$
0.040-0.070	$-.442 \pm 0.336 \pm 0.400$	$0.58 \pm 0.44 \pm 1.42$	$0.59 \pm 0.25 \pm 0.43$
0.070-0.100	$0.14 \pm 0.44 \pm 7.30$	$-.419 \pm 0.620 \pm 1.281$	$0.14 \pm 0.32 \pm 0.66$

Table 3. Results $R(y) = 1/\sigma \cdot d\sigma/dy$ at $\sqrt{s} = 172$, 183 and 189 GeV for the event shape observables y: oblateness O, C-parameter C, heavy jet mass M_H and sphericity S. The first error is statistical, the second systematic

O	$R(O)$ (172 GeV)		$R(O)$ (183 GeV)		$R(O)$ (189 GeV)	
0.000-0.050	10.6 ± 1.0	± 0.5	10.2 ± 0.5	± 0.4	9.97 ± 0.27	± 0.44
0.050-0.100	4.63 ± 0.68	± 0.71	4.30 ± 0.31	± 0.51	4.15 ± 0.18	± 0.38
0.100-0.150	1.93 ± 0.47	± 0.23	2.18 ± 0.23	± 0.25	2.33 ± 0.14	± 0.11
0.150-0.200	0.91 ± 0.34	± 0.23	1.32 ± 0.20	± 0.57	1.34 ± 0.12	± 0.23
0.200-0.250	0.46 ± 0.30	± 0.37	0.78 ± 0.16	± 0.47	0.82 ± 0.10	± 0.21
0.250-0.300	0.51 ± 0.29	± 0.19	0.72 ± 0.16	± 0.19	0.60 ± 0.09	± 0.18
0.300-0.400	0.28 ± 0.15	± 0.21	0.21 ± 0.07	± 0.09	0.29 ± 0.05	± 0.10
0.400-0.500	0.21 ± 0.11	± 0.15	0.031 ± 0.034	± 0.062	0.087 ± 0.028	± 0.057

C	$R(C)$ (172 GeV)		$R(C)$ (183 GeV)		$R(C)$ (189 GeV)	
0.000-0.050	2.76 ± 0.59	± 1.12	1.78 ± 0.22	± 0.33	1.82 ± 0.13	± 0.17
0.050-0.080	4.65 ± 0.92	± 2.48	5.70 ± 0.49	± 0.38	4.97 ± 0.26	± 0.19
0.080-0.110	4.68 ± 0.86	± 2.48	3.85 ± 0.37	± 0.60	4.21 ± 0.22	± 0.67
0.110-0.140	3.66 ± 0.73	± 0.86	3.31 ± 0.34	± 0.43	3.14 ± 0.19	± 0.47
0.140-0.180	2.12 ± 0.48	± 0.86	2.28 ± 0.24	± 0.33	2.45 ± 0.15	± 0.24
0.180-0.220	1.31 ± 0.39	± 0.48	1.77 ± 0.21	± 0.25	1.80 ± 0.13	± 0.28
0.220-0.300	1.62 ± 0.31	± 0.35	1.46 ± 0.14	± 0.13	1.27 ± 0.08	± 0.13
0.300-0.400	0.82 ± 0.21	± 0.21	0.80 ± 0.09	± 0.10	0.86 ± 0.06	± 0.08
0.400-0.500	0.28 ± 0.14	± 0.38	0.60 ± 0.09	± 0.20	0.66 ± 0.05	± 0.08
0.500-0.600	0.28 ± 0.15	± 0.26	0.44 ± 0.08	± 0.19	0.42 ± 0.05	± 0.14
0.600-0.750	0.45 ± 0.16	± 0.24	0.26 ± 0.07	± 0.09	0.35 ± 0.05	± 0.07
0.750-1.000	$-.002 \pm 0.057$	± 0.153	0.093 ± 0.058	± 0.102	0.082 ± 0.035	± 0.060

M_H	$R(M_H)$ (172 GeV)		$R(M_H)$ (183 GeV)		$R(M_H)$ (189 GeV)	
0.060-0.075	1.57 ± 0.53	± 1.32	1.20 ± 0.23	± 0.47	1.67 ± 0.17	± 0.23
0.075-0.090	5.52 ± 1.26	± 1.42	4.95 ± 0.57	± 0.98	4.35 ± 0.31	± 0.48
0.090-0.110	7.15 ± 1.37	± 2.60	6.31 ± 0.61	± 0.88	6.07 ± 0.34	± 0.56
0.110-0.140	5.84 ± 0.99	± 1.69	5.62 ± 0.48	± 0.63	6.42 ± 0.29	± 0.39
0.140-0.170	4.27 ± 0.84	± 1.44	5.06 ± 0.44	± 0.80	4.77 ± 0.25	± 0.35
0.170-0.200	4.03 ± 0.84	± 1.18	3.88 ± 0.39	± 0.66	3.22 ± 0.20	± 0.32
0.200-0.250	2.70 ± 0.54	± 0.50	2.71 ± 0.25	± 0.42	2.45 ± 0.14	± 0.15
0.250-0.300	0.88 ± 0.36	± 0.64	1.56 ± 0.21	± 0.14	1.66 ± 0.13	± 0.11
0.300-0.350	0.72 ± 0.34	± 0.21	1.08 ± 0.19	± 0.32	1.37 ± 0.13	± 0.19
0.350-0.450	0.56 ± 0.22	± 0.09	0.57 ± 0.11	± 0.04	0.57 ± 0.07	± 0.14
0.450-0.600	0.34 ± 0.13	± 0.19	0.11 ± 0.05	± 0.07	0.14 ± 0.03	± 0.10

S	$R(S)$ (172 GeV)		$R(S)$ (183 GeV)		$R(S)$ (189 GeV)	
0.000-0.020	26.7 ± 2.5	± 2.0	24.7 ± 1.1	± 2.0	25.0 ± 0.7	± 0.8
0.020-0.040	8.19 ± 1.43	± 1.60	7.70 ± 0.65	± 1.16	7.46 ± 0.38	± 0.69
0.040-0.060	3.63 ± 0.95	± 0.60	4.18 ± 0.51	± 0.71	4.15 ± 0.29	± 0.49
0.060-0.120	1.43 ± 0.39	± 0.26	2.04 ± 0.21	± 0.16	1.90 ± 0.12	± 0.12
0.120-0.200	0.60 ± 0.25	± 0.41	0.65 ± 0.12	± 0.17	0.79 ± 0.08	± 0.18
0.200-0.300	0.24 ± 0.19	± 0.22	0.44 ± 0.11	± 0.22	0.37 ± 0.07	± 0.04
0.300-0.500	0.17 ± 0.11	± 0.16	0.093 ± 0.060	± 0.093	0.22 ± 0.05	± 0.07
0.500-0.700	0.19 ± 0.12	± 0.25	0.16 ± 0.08	± 0.13	0.055 ± 0.030	± 0.046

Table 4. Results $R(y) = 1/\sigma \cdot d\sigma/dy$ at $\sqrt{s} = 172$, 183 and 189 GeV for the event shape observables y: total jet broadening B_T, wide jet broadening B_W and the transition value between 2- and 3-jets y_{23}^D. The first error is statistical, the second systematic

B_T	$R(B_T)$ (172 GeV)		$R(B_T)$ (183 GeV)		$R(B_T)$ (189 GeV)	
0.000-0.030	3.96 ± 0.98	± 1.68	1.40 ± 0.26	± 0.60	1.89 ± 0.17	± 0.36
0.030-0.040	11.3 ± 2.6	± 2.6	13.4 ± 1.3	± 2.0	9.84 ± 0.64	± 0.56
0.040-0.050	8.75 ± 2.09	± 7.73	12.9 ± 1.3	± 2.7	11.9 ± 0.7	± 1.7
0.050-0.060	11.7 ± 2.3	± 9.7	8.57 ± 0.91	± 1.54	9.59 ± 0.57	± 0.46
0.060-0.075	8.82 ± 1.59	± 2.61	8.69 ± 0.78	± 0.96	8.00 ± 0.42	± 0.53
0.075-0.090	4.46 ± 1.14	± 3.65	5.20 ± 0.58	± 0.99	6.33 ± 0.38	± 0.55
0.090-0.110	5.53 ± 1.12	± 1.06	5.67 ± 0.56	± 0.91	4.37 ± 0.27	± 0.61
0.110-0.130	3.19 ± 0.85	± 1.47	3.11 ± 0.40	± 0.64	3.88 ± 0.26	± 0.39
0.130-0.160	2.09 ± 0.59	± 0.92	2.64 ± 0.32	± 0.29	2.55 ± 0.18	± 0.24
0.160-0.200	1.21 ± 0.46	± 0.66	1.64 ± 0.24	± 0.29	1.75 ± 0.15	± 0.09
0.200-0.250	0.49 ± 0.35	± 0.45	0.93 ± 0.21	± 0.36	0.76 ± 0.13	± 0.47
0.250-0.300	1.11 ± 0.46	± 0.69	0.27 ± 0.20	± 0.38	0.66 ± 0.16	± 0.25
0.300-0.350	$-.002 \pm 0.345$	± 0.866	0.40 ± 0.30	± 0.52	0.058 ± 0.149	± 0.219

B_W	$R(B_W)$ (172 GeV)		$R(B_W)$ (183 GeV)		$R(B_W)$ (189 GeV)	
0.000-0.020	8.91 ± 1.75	± 3.96	4.81 ± 0.59	± 0.93	4.61 ± 0.34	± 0.91
0.020-0.030	14.5 ± 2.7	± 4.0	18.1 ± 1.5	± 1.0	16.8 ± 0.8	± 1.8
0.030-0.040	13.7 ± 2.4	± 4.5	13.1 ± 1.2	± 1.0	13.7 ± 0.7	± 0.5
0.040-0.050	8.48 ± 1.89	± 3.88	10.5 ± 1.0	± 0.4	10.3 ± 0.6	± 0.8
0.050-0.065	7.36 ± 1.49	± 2.67	8.23 ± 0.76	± 0.86	7.89 ± 0.43	± 0.42
0.065-0.080	6.41 ± 1.41	± 2.33	5.16 ± 0.61	± 1.06	5.44 ± 0.37	± 0.35
0.080-0.100	3.88 ± 1.01	± 1.43	4.51 ± 0.51	± 0.51	4.30 ± 0.30	± 0.32
0.100-0.150	1.57 ± 0.46	± 0.52	2.30 ± 0.26	± 0.38	2.66 ± 0.17	± 0.27
0.150-0.200	1.02 ± 0.43	± 0.31	1.25 ± 0.24	± 0.28	1.03 ± 0.13	± 0.24
0.200-0.250	0.77 ± 0.35	± 0.39	0.33 ± 0.14	± 0.21	0.53 ± 0.11	± 0.23
0.250-0.300	0.048 ± 0.099	± 0.331	0.014 ± 0.058	± 0.195	0.048 ± 0.038	± 0.074

| y_{23}^D	$R(y_{23}^D)$ (172 GeV)		$R(y_{23}^D)$ (183 GeV)		$R(y_{23}^D)$ (189 GeV)	
0.00030-0.00075	$399. \pm 70.$	$\pm 139.$	$335. \pm 31.$	$\pm 56.$	$348. \pm 18.$	$\pm 56.$
0.00075-0.00130	$202. \pm 42.$	$\pm 40.$	$215. \pm 21.$	$\pm 25.$	$163. \pm 10.$	$\pm 31.$
0.00130-0.00230	84.5 ± 19.7	± 41.5	$101. \pm 10.$	$\pm 9.$	$111. \pm 6.$	$\pm 10.$
0.00230-0.00400	56.4 ± 12.1	± 24.6	56.3 ± 5.9	± 9.8	62.5 ± 3.6	± 7.5
0.00400-0.00700	34.0 ± 7.2	± 5.6	29.7 ± 3.2	± 5.1	29.7 ± 1.9	± 6.4
0.00700-0.01200	16.8 ± 4.2	± 6.0	18.7 ± 2.1	± 5.4	16.6 ± 1.1	± 2.6
0.01200-0.02300	8.20 ± 2.10	± 1.99	7.77 ± 0.96	± 1.50	9.01 ± 0.61	± 1.14
0.02300-0.04000	2.56 ± 0.98	± 1.74	4.67 ± 0.60	± 1.06	4.21 ± 0.35	± 0.96
0.04000-0.07000	2.46 ± 0.73	± 1.47	1.74 ± 0.30	± 0.62	1.98 ± 0.19	± 0.25
0.07000-0.13000	0.19 ± 0.24	± 1.02	0.72 ± 0.16	± 0.28	0.76 ± 0.10	± 0.08
0.13000-0.23500	0.45 ± 0.19	± 0.28	0.19 ± 0.07	± 0.08	0.27 ± 0.05	± 0.10
0.23500-0.40000	0.036 ± 0.048	± 0.074	0.050 ± 0.054	± 0.111	0.014 ± 0.018	± 0.037
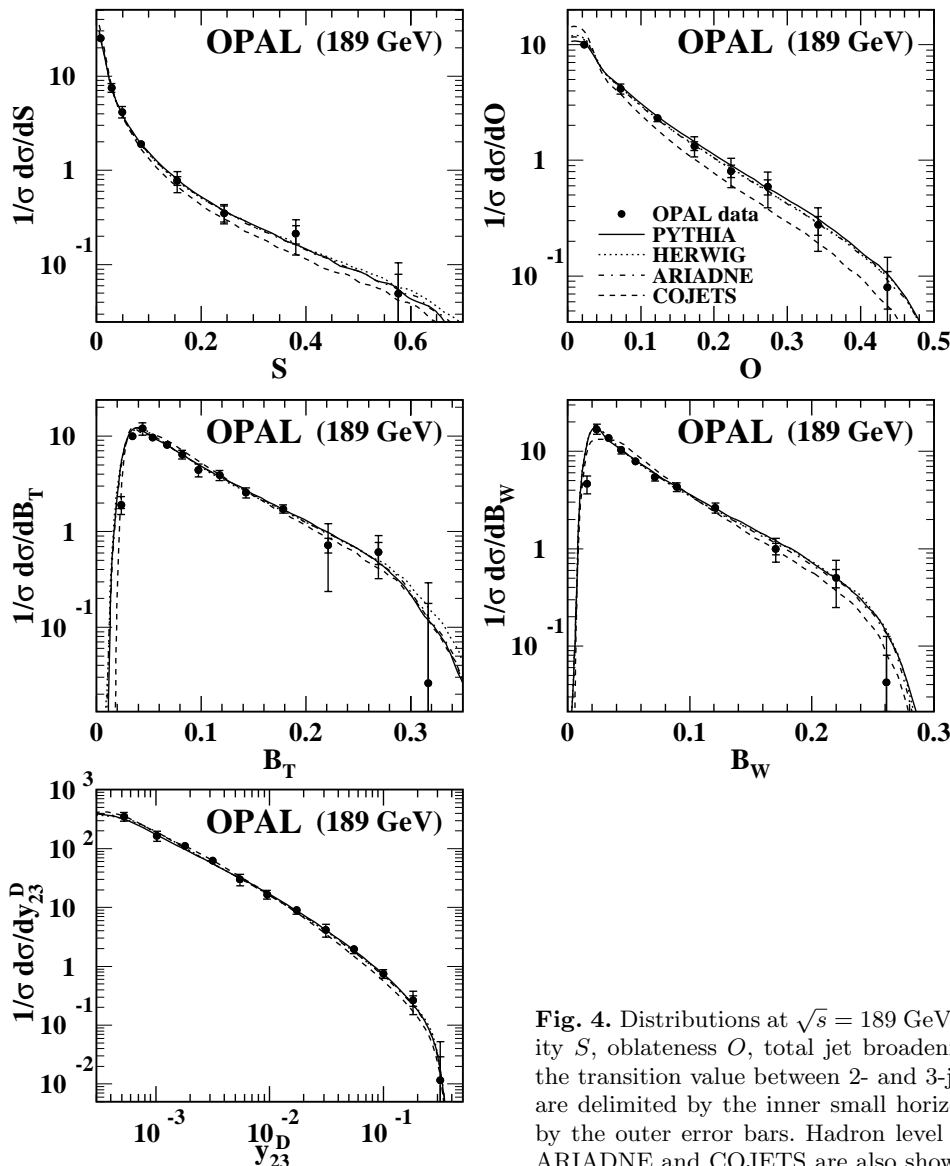
Fig. 4. Distributions at $\sqrt{s} = 189$ GeV of the event shape observables sphericity S, oblateness O, total jet broadening B_T, wide jet broadening B_W, and the transition value between 2- and 3-jets y_{23}^D. Experimental statistical errors are delimited by the inner small horizontal bars. The total errors are shown by the outer error bars. Hadron level predictions from PYTHIA, HERWIG, ARIADNE and COJETS are also shown

ARIADNE and HERWIG. The COJETS Monte Carlo model deviates from the data for T_{minor}, M_H and O, but describes the remaining event shapes reasonably well. Note that all generators have been tuned at $\sqrt{s} = M_{Z^0}$, and are not re-tuned at these higher energies.

The mean value of the thrust distribution, $\langle T \rangle$, as a function of the c.m. energy, is shown in Fig. 5 together with data from lower energy measurements [1, 2, 25, 41] and the predictions for the energy evolution from PYTHIA, HERWIG, ARIADNE and COJETS. The predictions of all four Monte Carlo models are consistent with our new measurements.
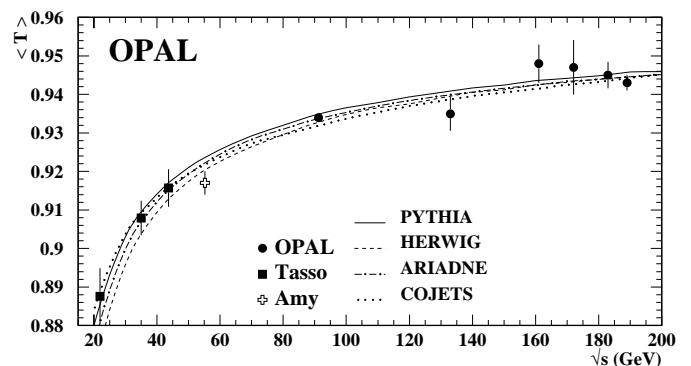

Fig. 5. Distribution of the mean thrust $\langle T \rangle$ as a function of the centre-of-mass energy, compared to several QCD models

5.2 Determination of α_s

Our measurement of the strong coupling strength $\alpha_s(\mathrm{Q})$ is based on fits of the QCD predictions to the corrected distributions for $1 - T$, M_H, C, B_T, B_W and y_{23}^D. The theoretical descriptions of these six observables are the most complete, allowing the use of combined $\mathcal{O}(\alpha_s^2) + \mathrm{NLLA}$ QCD calculations [40, 42–45]. We follow the procedures described
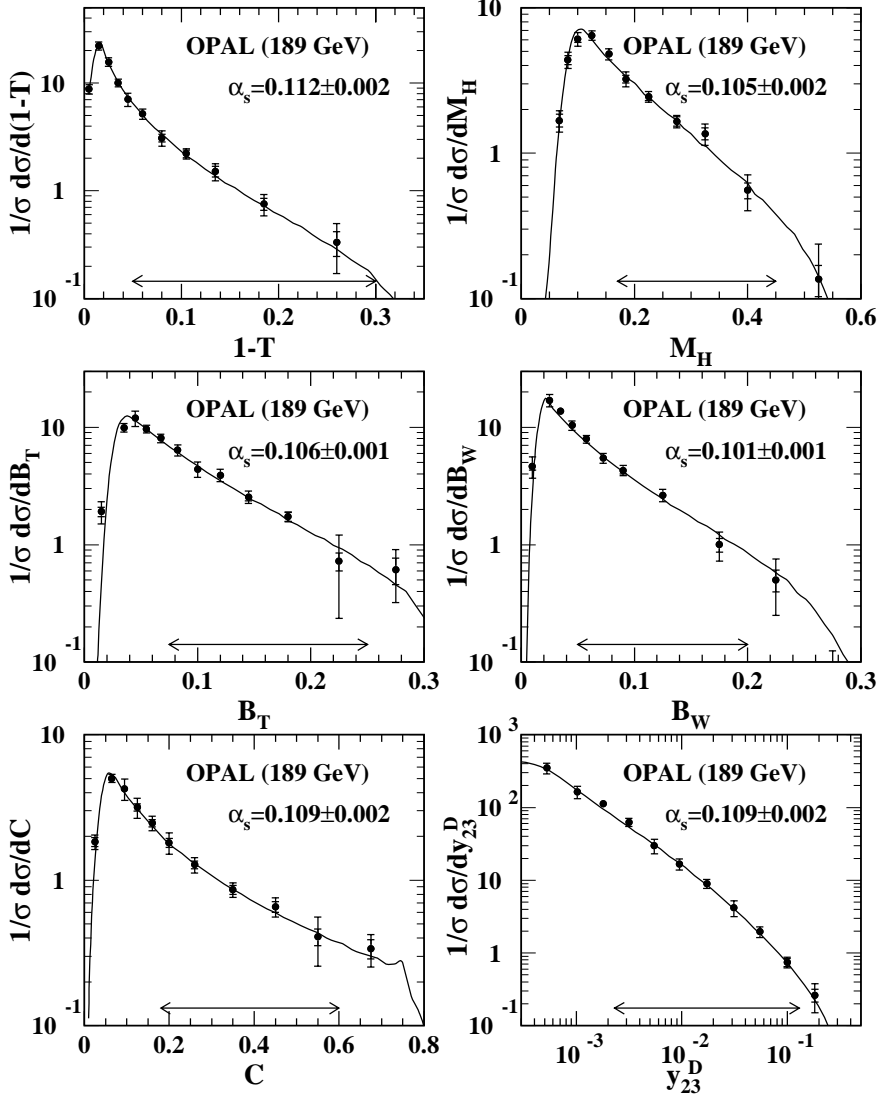
Fig. 6. Distributions of the event shape observables thrust $1 - T$, heavy jet mass M_H, total B_T and wide B_W jet broadening, C-parameter and the transition value between 2- and 3-jets y_{23}^D, are shown together with fits of the $\mathcal{O}(\alpha_s^2)$+NLLA QCD predictions, with α_s as fitted parameter. The fitted regions are indicated by the arrows
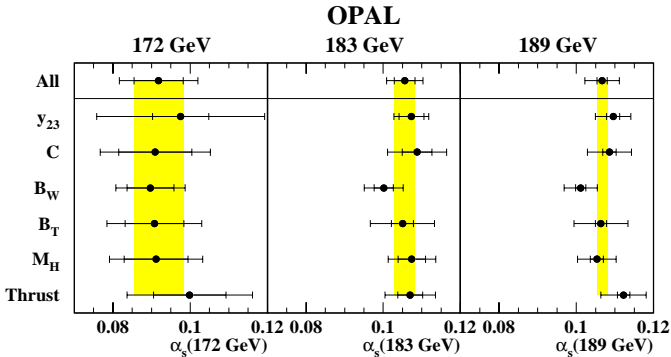

Fig. 7. Fitted values of α_s for each event shape at 172, 183 and 189 GeV. The inner error bar is statistical, the outer corresponds to the total systematic uncertainty. The light band corresponds to the statistical uncertainty of α_s obtained as the weighted mean

sis. In particular, we choose the so-called $\ln(R)$-matching scheme, and fix the renormalization scale parameter, $x_\mu \equiv \mu/\sqrt{s}$, to $x_\mu = 1$, where μ is the energy scale at which the theory is renormalised. The $\mathcal{O}(\alpha_s^2)$+NLLA prediction for C has only recently become available [45], and was not used in our earlier publications.

Analytic QCD predictions describe distributions at the level of quarks and gluons (parton level). The predictions are convoluted with hadronization effects by multiplying by the ratio of hadron- to parton level distributions determined using a Monte Carlo model. We use PYTHIA to generate events at $\sqrt{s} = 172$, 183 and 189 GeV for this purpose.

The fit ranges are determined by the following considerations. For each observable, the ratio between Monte Carlo distributions computed for partons and hadrons is required to be unity to within about 10% and the distribution of partons from Monte Carlo models is required to be described well by the analytic predictions. The fit ranges are identical to the fit ranges used in our studies at $\sqrt{s} = M_{Z^0}$, 130 and 161 GeV [25,1,2].

in [25,1] as closely as possible in order to obtain results which we can compare directly to our previous analy-

Table 5. Values of $\alpha_s(172\ \text{GeV})$, $\alpha_s(183\ \text{GeV})$ and $\alpha_s(189\ \text{GeV})$ derived using the $\mathcal{O}(\alpha_s^2)$+NLLA QCD calculations with $x_\mu = 1$ and the $\ln(R)$-matching scheme, fit ranges and $\chi^2/\text{d.o.f.}$ values for each of the six event shape observables. In addition, the statistical, and various systematic uncertainties are given. The sign indicates the direction in which α_s changes with respect to the standard analysis

172 GeV	$1-T$	M_H	B_T	B_W	C	y_{23}^D	Mean
fit range	0.05-0.30	0.17-0.45	0.075-0.25	0.05-0.20	0.18-0.60	0.0023-0.130	-
α_s	0.0999	0.0912	0.0908	0.0897	0.0910	0.0976	0.0919
χ^2/dof	6.7/5	5.0/4	3.3/5	2.7/4	5.9/4	7.9/6	-
Stat	±0.0094	±0.0083	±0.0076	±0.0061	±0.0095	±0.0073	±0.0064
Exp	±0.0127	±0.0084	±0.0085	±0.0061	±0.0100	±0.0203	±0.0074
Hadr	±0.0019	±0.0016	±0.0032	±0.0014	±0.0023	±0.0028	±0.0015
$x_\mu = 0.5$	−0.0030	−0.0015	−0.0029	−0.0018	−0.0024	+0.0000	−0.0020
$x_\mu = 2$	+0.0038	+0.0023	+0.0036	+0.0025	+0.0031	+0.0016	+0.0028
Syst	±0.0133	±0.0087	±0.0096	±0.0066	±0.0106	±0.0205	±0.0079
Total	±0.0163	±0.0121	±0.0123	±0.0090	±0.0142	±0.0217	±0.0102

183 GeV	$1-T$	M_H	B_T	B_W	C	y_{23}^D	Mean
fit range	0.05-0.30	0.17-0.45	0.075-0.25	0.05-0.20	0.18-0.60	0.0023-0.130	-
α_s	0.1070	0.1074	0.1050	0.1001	0.1088	0.1073	0.1056
χ^2/dof	3.6/5	2.9/4	6.8/5	2.8/4	1.8/4	3.0/6	-
Stat	±0.0032	±0.0036	±0.0029	±0.0025	±0.0039	±0.0032	±0.0027
Exp	±0.0033	±0.0032	±0.0056	±0.0027	±0.0042	±0.0024	±0.0019
Hadr	±0.0015	±0.0017	±0.0021	±0.0008	±0.0016	±0.0016	±0.0010
$x_\mu = 0.5$	−0.0038	−0.0028	−0.0045	−0.0030	−0.0043	−0.0004	−0.0026
$x_\mu = 2$	+0.0048	+0.0040	+0.0055	+0.0038	+0.0054	+0.0024	+0.0039
Syst	±0.0056	±0.0050	±0.0078	±0.0044	±0.0066	±0.0032	±0.0039
Total	±0.0065	±0.0062	±0.0083	±0.0051	±0.0077	±0.0045	±0.0047

189 GeV	$1-T$	M_H	B_T	B_W	C	y_{23}^D	Mean
fit range	0.05-0.30	0.17-0.45	0.075-0.25	0.05-0.20	0.18-0.60	0.0023-0.130	-
α_s	0.1122	0.1053	0.1064	0.1011	0.1086	0.1095	0.1067
χ^2/dof	2.0/5	5.1/4	7.6/5	5.1/4	1.7/4	6.4/6	-
Stat	±0.0016	±0.0017	±0.0014	±0.0013	±0.0018	±0.0017	±0.0013
Exp	±0.0021	±0.0027	±0.0041	±0.0020	±0.0019	±0.0036	±0.0021
Hadr	±0.0013	±0.0018	±0.0020	±0.0008	±0.0014	±0.0017	±0.0008
$x_\mu = 0.5$	−0.0045	−0.0029	−0.0047	−0.0031	−0.0044	−0.0004	−0.0030
$x_\mu = 2$	+0.0056	+0.0040	+0.0056	+0.0040	+0.0054	+0.0026	+0.0043
Syst	±0.0056	±0.0047	±0.0069	±0.0041	±0.0054	±0.0043	±0.0043
Total	±0.0058	±0.0050	±0.0070	±0.0043	±0.0057	±0.0046	±0.0045

We find satisfactory fits for all six observables, for all three c.m. energies. In particular, the C distributions are well described by the newly introduced predictions. In Table 5 we quote the result on $\alpha_s(172\ \text{GeV})$, $\alpha_s(183\ \text{GeV})$ and $\alpha_s(189\ \text{GeV})$ for all six observables. In Fig. 6 we show the results for the determination of $\alpha_s(189\ \text{GeV})$. Note also that outside the fit ranges the data agree with the $\mathcal{O}(\alpha_s^2)$+NLLA predictions.

For each observable, the statistical uncertainties are estimated from the variance of α_s values derived from fits to 100 independent sets of simulated events, each with the same number of events as the data.

We also derive a combined result of the six observables for the strong coupling strength using the weighted average procedure as described in [25], which includes the correlations between the shapes. The statistical uncertainty of the combined result is estimated using 100 independent samples of Monte Carlo events in the same manner as for the individual measurements.

Table 6. Weighted mean values of α_s, derived from fits to six event shapes using the $\mathcal{O}(\alpha_s^2)$+NLLA QCD calculations with $x_\mu = 1$ and the $\ln(R)$-matching scheme, for c.m. energies at 172, 183 and 189 GeV. Full detailed breakdown of the systematic uncertainties are listed. The sign indicates the direction in which α_s changes with respect to the standard analysis. The last column correspond to the values of α_s, constructed at the luminosity weighted mean c.m. energy

	172 GeV	183 GeV	189 GeV	187 GeV
$\alpha_s(Q)$	0.0919	0.1056	0.1067	0.1060
Statistical error	± 0.0064	± 0.0027	± 0.0013	± 0.0012
Tracks+Clusters	-0.0017	$+0.0004$	$+0.0005$	$+0.0004$
Tracks Only	$+0.0019$	$+0.0008$	$+0.0019$	$+0.0017$
$|\cos\theta_T| < 0.7$	-0.0049	$+0.0002$	-0.0003	-0.0003
Alternative $\sqrt{s'}$	$+0.0035$	$+0.0012$	$+0.0007$	$+0.0009$
W_{QCD}	$+0.0024$	$+0.0012$	$+0.0003$	$+0.0002$
Background $\pm 5\%$	$+0.0004$	$+0.0002$	$+0.0002$	$+0.0002$
Experimental syst.	± 0.0074	± 0.0019	± 0.0021	± 0.0020
$b - 1$ s.d.	-0.0001	-0.0001	-0.0001	-0.0001
$b + 1$ s.d.	$+0.0001$	$+0.0001$	$+0.0001$	$+0.0001$
$\sigma_q - 1$ s.d.	$+0.0002$	$+0.0001$	$+0.0001$	$+0.0001$
$\sigma_q + 1$ s.d.	-0.0002	-0.0001	-0.0001	-0.0001
$Q_0 = 4$ GeV	$+0.0001$	$+0.0004$	$+0.0003$	$+0.0003$
udsc only	$+0.0010$	$+0.0003$	$+0.0002$	$+0.0003$
HERWIG 5.9	-0.0006	-0.0003	-0.0002	-0.0003
ARIADNE 4.08	$+0.0009$	$+0.0007$	$+0.0007$	$+0.0007$
Total hadronisation	± 0.0015	± 0.0010	± 0.0008	± 0.0009
$x_\mu = 0.5$	-0.0020	-0.0026	-0.0030	-0.0029
$x_\mu = 2$	$+0.0028$	$+0.0039$	$+0.0043$	$+0.0041$
Tot. syst. error	± 0.0079	± 0.0039	± 0.0043	± 0.0041

Table 7. Weighted mean values of α_s, as determined in Table 6, evolved to M_{Z^0}

	172 GeV	183 GeV	189 GeV	187 GeV
$\alpha_s(M_{\mathrm{Z}^0})$	0.0992	0.1165	0.1183	0.1173
Statistical error	± 0.0072	± 0.0033	± 0.0016	± 0.0015
Total error	± 0.0120	± 0.0057	± 0.0056	± 0.0053

The experimental uncertainty is estimated by adding in quadrature the following contributions: the largest difference between the central result and the results from tracks and all clusters or tracks only; the difference found when using the alternative $\sqrt{s'}$ selection; the difference when requiring the thrust axis to lie in the range $|\cos\theta_T| < 0.7$; the difference from using the variation on W_{QCD} to reject 4-fermion events; and the difference when the 4-fermion background is scaled by $\pm 5\%$. The experimental uncertainties, shown for each observable in Table 5, are of similar size as the statistical uncertainties. In Table 6 we present details of the experimental uncertainty for the weighted mean value of α_s, at each c.m. energy.

The hadronization uncertainty is defined by adding in quadrature: the larger of the changes in α_s observed when varying the hadronization parameters b and σ_Q by ± 1 standard deviation about their tuned values [15] in PYTHIA; the change observed when the parton virtuality cutoff parameter is altered from $Q_0 = 1.9$ GeV to $Q_0 = 4$ GeV in PYTHIA (without changing the other Monte Carlo parameters), corresponding to a change of the mean parton multiplicity from 7.4 to 5.0; the change observed when at the parton level only the light quarks
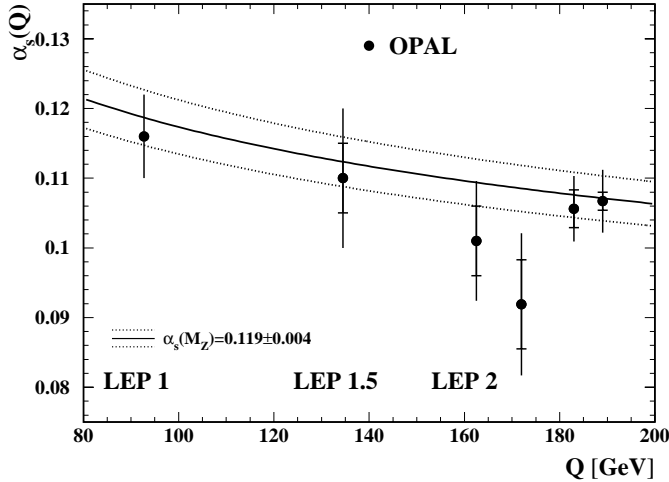
Fig. 8. Values of α_s, as determined from fits to $1-T$, M_H, B_T and B_W, as function of energy, on a linear scale. The curves show the $\mathcal{O}(\alpha_s^3)$ QCD prediction for $\alpha_s(Q)$ using $\alpha_s(M_{Z^0}) = 0.119 \pm 0.004$ [46]; the full line shows the central value while the dotted lines indicate the variation given by the uncertainty
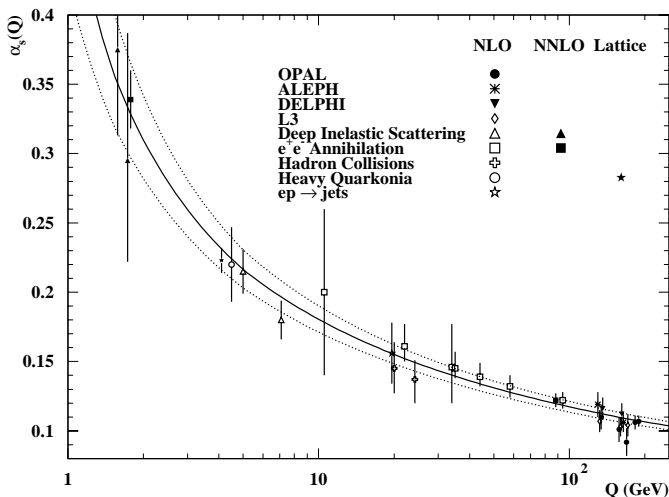

Fig. 9. Values of α_s as function of energy [46]. The labels NLO and NNLO refer to the order of calculation used. NLO corresponds to $\mathcal{O}(\alpha_s^2)$ in e⁺e⁻ annihilations, and NNLO to $\mathcal{O}(\alpha_s^3)$. The label Lattice refers to α_s values determined from lattice QCD calculations. The curves show the $\mathcal{O}(\alpha_s^3)$ QCD prediction for $\alpha_s(Q)$ using $\alpha_s(M_{Z^0}) = 0.119 \pm 0.004$; the full line shows the central value while the dotted lines indicate the variation given by the uncertainty

u, d, s and c are considered in order to estimate potential quark mass effects; and both differences with respect to the standard result when HERWIG or ARIADNE are used to account for the hadronization effects, rather than PYTHIA. For all observables the hadronization uncertainties are given in Table 5. These uncertainties are relatively small compared to the statistical uncertainty of α_s for the 172 GeV sample, but become of similar size to the statistical uncertainty for the 189 GeV sample. In Table 6

we show the individual contributions to the hadronization uncertainty for the weighted mean value of α_s.

The importance of uncomputed higher order terms in the theory may be estimated by studying the effects of varying the renormalization scale parameter x_μ. We estimate the dependence of our fit results on the renormalization scale x_μ as in [25,1], by repeating the fits using $x_\mu = 0.5$ and $x_\mu = 2$. We define the average deviation from the central result as the systematic uncertainty. We find variations which are generally larger than any other systematic variation and which are highly correlated between all observables[2].

As discussed in [25], we assign no additional systematic error resulting from the choice of the $\ln(R)$-matching scheme. Differences between the results for this and alternative matching schemes relate to missing higher order terms and are accounted for already by the variation of the renormalization scale x_μ.

The total uncertainty for each individual observable is computed by adding in quadrature the statistical, experimental, hadronization and scale uncertainties. The total uncertainty on α_s is typically around 10% at $\sqrt{s} = 172$ GeV and around 5% at $\sqrt{s} = 183$ and $\sqrt{s} = 189$ GeV.

As a consistency check we repeated the fits to α_s while varying the fit ranges. The fit range was changed by plus or minus one bin at either side. In general the observed deviations to the central value of α_s were small and we do not include this check in our systematic uncertainty.

Our result for the computed average of the six event shapes, each weighted with its total uncertainty, is

$$\alpha_s(172 \text{ GeV}) = 0.092 \pm 0.006(\text{stat.}) \pm 0.008(\text{syst.}),$$
$$\alpha_s(183 \text{ GeV}) = 0.106 \pm 0.003(\text{stat.}) \pm 0.004(\text{syst.}), \quad (3)$$
$$\alpha_s(189 \text{ GeV}) = 0.107 \pm 0.001(\text{stat.}) \pm 0.004(\text{syst.}).$$

The systematic uncertainty has contributions from experimental effects $\pm(0.002 - 0.007)$, hadronization effects $\pm(0.001 - 0.002)$ and from variations of the renormalization scale $\pm(0.002 - 0.004)$, as explained above. The systematic variations of the combined results are detailed in Table 6. Their values evolved to M_{Z^0} are listed in Table 7. In Fig. 7 we show the values of α_s we obtain from all event shapes at the three energies. In the same figure we also show the computed weighted averages of α_s. The spread in the values of α_s as obtained from the six event shapes is small, and the computed weighted average of α_s covers the individual measurements within the uncertainty. Note however that α_s determined using B_W at 183 and 189 GeV is somewhat smaller, as already observed at LEP-1 energies [25], which may indicate that the higher order corrections to B_W are slightly different from those of the other event shapes.

The correlations between the values of α_s at the three different c.m. energies are large. For example, the correlations between the theoretical uncertainties of the three

---
[2] The compensation in α_s due to a change of the renormalisation scale x_μ in the QCD predictions is proportional to the value of α_s itself. The scale uncertainty at our 172 GeV sample is therefore smaller than that at 183 or 189 GeV, where the value for α_s we obtain is larger.
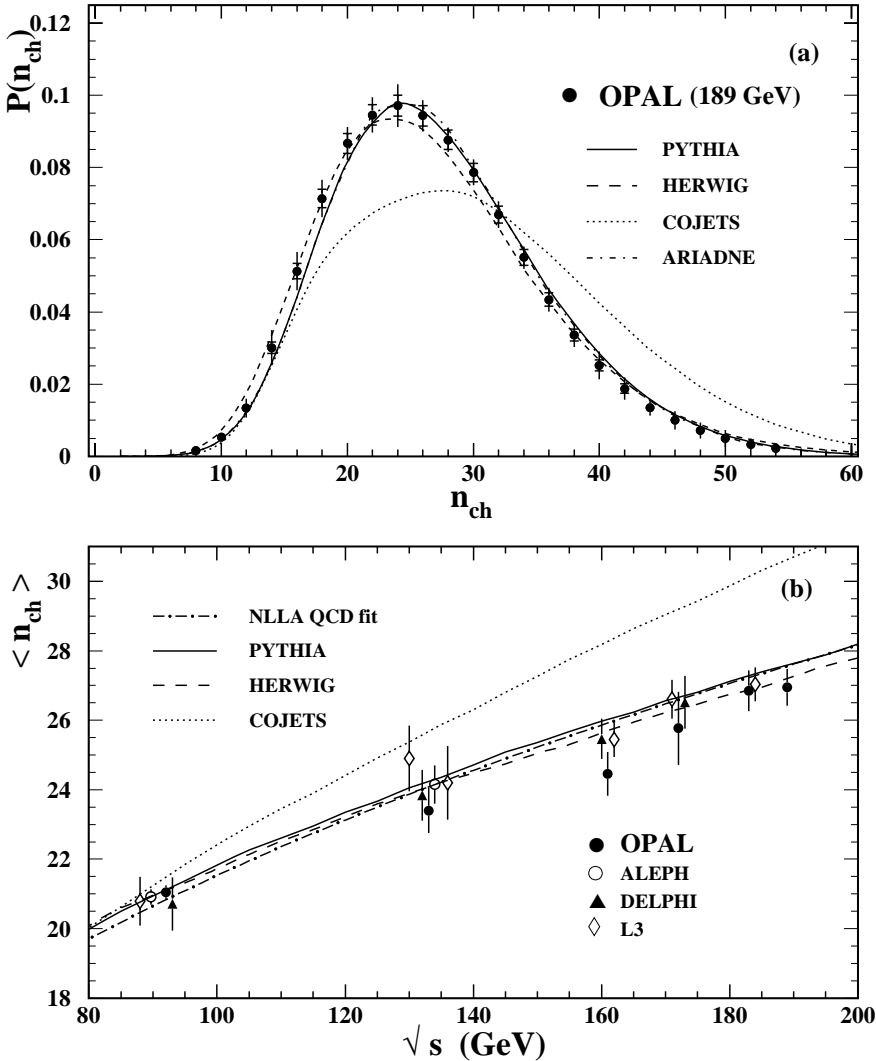
Fig. 10. a Corrected distribution of the charged particle multiplicity n_{ch}. b Mean charged multiplicity measurements by LEP experiments over a range of $\sqrt{s}$ from 91.2 GeV to 189 GeV. The NLLA QCD prediction for the evolution of charged particle multiplicity with $\sqrt{s}$ uses all data points available from 12 GeV up to 161 GeV. Also shown are the predictions from PYTHIA, HERWIG, and CO-JETS. In b the curve for the ARIADNE prediction is almost indistinguishable from the PYTHIA prediction and is omitted. Note that the systematic uncertainties on the OPAL measurements at energies $\sqrt{s} >$ 91.2 GeV are highly correlated

values of α_s quoted in equation 3, are all close to 100%. The correlation coefficients for the experimental uncertainties vary between 40% and 67%, and the ones for the hadronization corrections vary between 84% and 98%.

In order to allow for the effects of these correlations, we construct a value of α_s at the scale given by the luminosity weighted c.m. energy of our three data samples, 186.7 GeV. We use $\mathcal{O}(\alpha_s^3)$ predictions to evolve all our values of α_s to this scale. As a final result, using the weighted mean values of α_s at all three energies, we obtain

$$\alpha_s(187 \text{ GeV}) = 0.106 \pm 0.001(\text{stat.}) \pm 0.004(\text{syst.}). \quad (4)$$

When evolved to the scale of M_{Z^0}, using $\mathcal{O}(\alpha_s^3)$ calculations, the value of the weighted average for α_s becomes $\alpha_s(M_{Z^0}) = 0.117 \pm 0.005$ (see also Table 7). For comparison, our measurements at the M_{Z^0} energy with a slightly different set of observables based on $\mathcal{O}(\alpha_s^2)$+NLLA QCD calculations yielded $\alpha_s(M_{Z^0}) = 0.120 \pm 0.006$ [25].

In order to compare average α_s values using exactly the same theoretical predictions and observables as used in our previous publications, we compute the weighted average from our present fits to only $1 - T$, M_H, B_T and B_W. This is $\alpha_s(187 \text{ GeV}) = 0.104 \pm 0.005$ which corresponds to $\alpha_s(M_{Z^0}) = 0.115 \pm 0.006$ when evolved to the scale of M_{Z^0}. Our previous analysis at $\sqrt{s} = M_{Z^0}$ gave $\alpha_s(M_{Z^0}) = 0.116 \pm 0.006$ from fits of the same predictions to the same observables. Our present determinations of α_s are therefore consistent with our measurement at $\sqrt{s} = M_{Z^0}$.

In Fig. 8 we show our result (3) together with our other measurements of the strong coupling strength, as a function of the energy scale Q. The curve shows the $\mathcal{O}(\alpha_s^3)$ prediction for $\alpha_s(Q)$ using $\alpha_s(M_{Z^0}) = 0.119 \pm 0.004$, the value of $\alpha_s(M_{Z^0})$ as given in [46]. Note that this value of α_s is obtained using many observables, from a wide variety of experimental environments. Our determinations of α_s, obtained with the four event shapes mentioned above, all fall below the predictions of [46]. This indicates that the values obtained using these observables are somewhat shifted with respect to the value from [46]. However, the consistency of our measurements between the LEP-1 and LEP-2 c.m. energies is excellent.

Table 8. Charged particle multiplicity in percent, measured at $\sqrt{s} = 172$, 183 and 189 GeV. The first error is statistical, the second systematic

n_{ch}	P(n_{ch}) 172 GeV [%]			P(n_{ch}) 183 GeV [%]			P(n_{ch}) 189 GeV [%]		
8.	.24 $\pm$	.19 $\pm$	.28	.09 $\pm$	.05 $\pm$	.08	.17 $\pm$	.03 $\pm$	.05
10.	.68 $\pm$	.38 $\pm$	.42	.35 $\pm$	.08 $\pm$	.13	.54 $\pm$	.06 $\pm$	.12
12.	1.31 $\pm$	.34 $\pm$	.61	1.17 $\pm$	.16 $\pm$	.18	1.34 $\pm$	.10 $\pm$	.27
14.	3.72 $\pm$	.70 $\pm$	.78	2.54 $\pm$	.26 $\pm$	.26	3.01 $\pm$	.16 $\pm$	.40
16.	5.81 $\pm$	.83 $\pm$	1.01	4.96 $\pm$	.36 $\pm$	.49	5.13 $\pm$	.21 $\pm$	.47
18.	8.29 $\pm$	1.01 $\pm$	1.31	7.67 $\pm$	.47 $\pm$	.69	7.15 $\pm$	.26 $\pm$	.44
20.	10.30 $\pm$	1.13 $\pm$	1.15	9.57 $\pm$	.52 $\pm$	.72	8.67 $\pm$	.28 $\pm$	.41
22.	10.12 $\pm$	1.02 $\pm$	.98	10.40 $\pm$	.53 $\pm$	.56	9.46 $\pm$	.28 $\pm$	.43
24.	10.32 $\pm$	1.05 $\pm$	.78	10.35 $\pm$	.53 $\pm$	.47	9.72 $\pm$	.29 $\pm$	.42
26.	9.10 $\pm$	.92 $\pm$	.86	9.68 $\pm$	.49 $\pm$	.51	9.44 $\pm$	.28 $\pm$	.36
28.	9.13 $\pm$	.99 $\pm$	.85	8.59 $\pm$	.45 $\pm$	.60	8.77 $\pm$	.27 $\pm$	.26
30.	7.73 $\pm$	.88 $\pm$	.76	7.30 $\pm$	.43 $\pm$	.66	7.87 $\pm$	.25 $\pm$	.25
32.	6.32 $\pm$	.79 $\pm$	.75	6.00 $\pm$	.37 $\pm$	.55	6.70 $\pm$	.23 $\pm$	.25
34.	5.01 $\pm$	.69 $\pm$	.83	4.81 $\pm$	.34 $\pm$	.37	5.51 $\pm$	.22 $\pm$	.26
36.	3.69 $\pm$	.57 $\pm$	.97	3.80 $\pm$	.32 $\pm$	.27	4.34 $\pm$	.19 $\pm$	.26
38.	2.42 $\pm$	.44 $\pm$	.86	3.13 $\pm$	.31 $\pm$	.25	3.36 $\pm$	.17 $\pm$	.30
40.	1.71 $\pm$	.37 $\pm$	.68	2.61 $\pm$	.30 $\pm$	.26	2.52 $\pm$	.15 $\pm$	.31
42.	1.19 $\pm$	.31 $\pm$	.45	2.11 $\pm$	.27 $\pm$	.21	1.88 $\pm$	.13 $\pm$	.27
44.	.55 $\pm$	.16 $\pm$	.26	1.61 $\pm$	.26 $\pm$	.19	1.35 $\pm$	.12 $\pm$	.24
46.	.36 $\pm$	.16 $\pm$	.22	1.15 $\pm$	.27 $\pm$	.14	1.00 $\pm$	.12 $\pm$	.21
48.	.30 $\pm$	.25 $\pm$	.26	.88 $\pm$	.21 $\pm$	.16	.72 $\pm$	.11 $\pm$	.21
50.	.35 $\pm$	.38 $\pm$	.30	.56 $\pm$	.22 $\pm$	.21	.50 $\pm$	.10 $\pm$	.18
52.	.07 $\pm$	.07 $\pm$	.29	.32 $\pm$	.22 $\pm$	.24	.34 $\pm$	.09 $\pm$	.16
54.	.01 $\pm$	.02 $\pm$	.28	.19 $\pm$	.11 $\pm$	.19	.21 $\pm$	.09 $\pm$	.12
56.	.02 $\pm$	.04 $\pm$	.31	.14 $\pm$	.12 $\pm$	.14	.12 $\pm$	.06 $\pm$	.09
58.	.26 $\pm$	.39 $\pm$	.25	.00 $\pm$	.00 $\pm$	.12	.06 $\pm$	.04 $\pm$	.11
60.	.01 $\pm$	.03 $\pm$	.72	.03 $\pm$	.04 $\pm$	.13	.09 $\pm$	.10 $\pm$	.09
62.	.01 $\pm$	.02 $\pm$	.28	.00 $\pm$	.00 $\pm$	.13	.02 $\pm$	.06 $\pm$	.09
$\langle n_{ch} \rangle$	25.77 $\pm$	0.58 $\pm$	0.88	26.85 $\pm$	0.27 $\pm$	0.52	26.95 $\pm$	0.16 $\pm$	0.51
D	8.38 $\pm$	0.63 $\pm$	1.29	8.36 $\pm$	0.20 $\pm$	0.46	8.45 $\pm$	0.12 $\pm$	0.34
$\langle n_{ch} \rangle / D$	3.08 $\pm$	0.21 $\pm$	0.45	3.21 $\pm$	0.07 $\pm$	0.14	3.19 $\pm$	0.04 $\pm$	0.09
C_2	1.106 $\pm$	0.014 $\pm$	0.030	1.097 $\pm$	0.004 $\pm$	0.017	1.098 $\pm$	0.003 $\pm$	0.005
$\mathcal{R}_2$	1.067 $\pm$	0.014 $\pm$	0.031	1.060 $\pm$	0.004 $\pm$	0.017	1.061 $\pm$	0.003 $\pm$	0.006

We obtained a relatively low value of α_s using the 172 GeV sample alone for all event shape observables; approximately 1.8 standard deviations below expectations.

In Fig. 9 we show our results again, on a logarithmic scale, together with results obtained from the other experiments at lower c.m. energies.

5.3 Charged multiplicity

We measure the charged particle multiplicity distribution and derive several related quantities from it, in particular the mean charged multiplicity $\langle n_{ch} \rangle$, the dispersion $D = (\langle n_{ch}^2 \rangle - \langle n_{ch} \rangle^2)^{\frac{1}{2}}$, the ratio $\langle n_{ch} \rangle / D$, the normalised

second moment $C_2 = \langle n_{ch}^2 \rangle / \langle n_{ch} \rangle^2$ and the second binomial moment [2] $\mathcal{R}_2 = \langle n_{ch}(n_{ch} - 1) \rangle / \langle n_{ch} \rangle^2$.

To correct the observed charged particle multiplicity distribution, we first subtract the expected background from 4-fermion events as described in Sect. 4. The resulting distribution is corrected for experimental effects such as acceptance, resolution and secondary interactions in the detector with an unfolding matrix, as previously done in [1,47]. This matrix is determined from the PYTHIA sample of fully simulated $(Z^0/\gamma)^*$ events. Biases introduced by the event selection, by radiative events passing the selection and by the fraction of particles with lifetimes shorter than 3×10^{-10} s that did not decay in the detector are
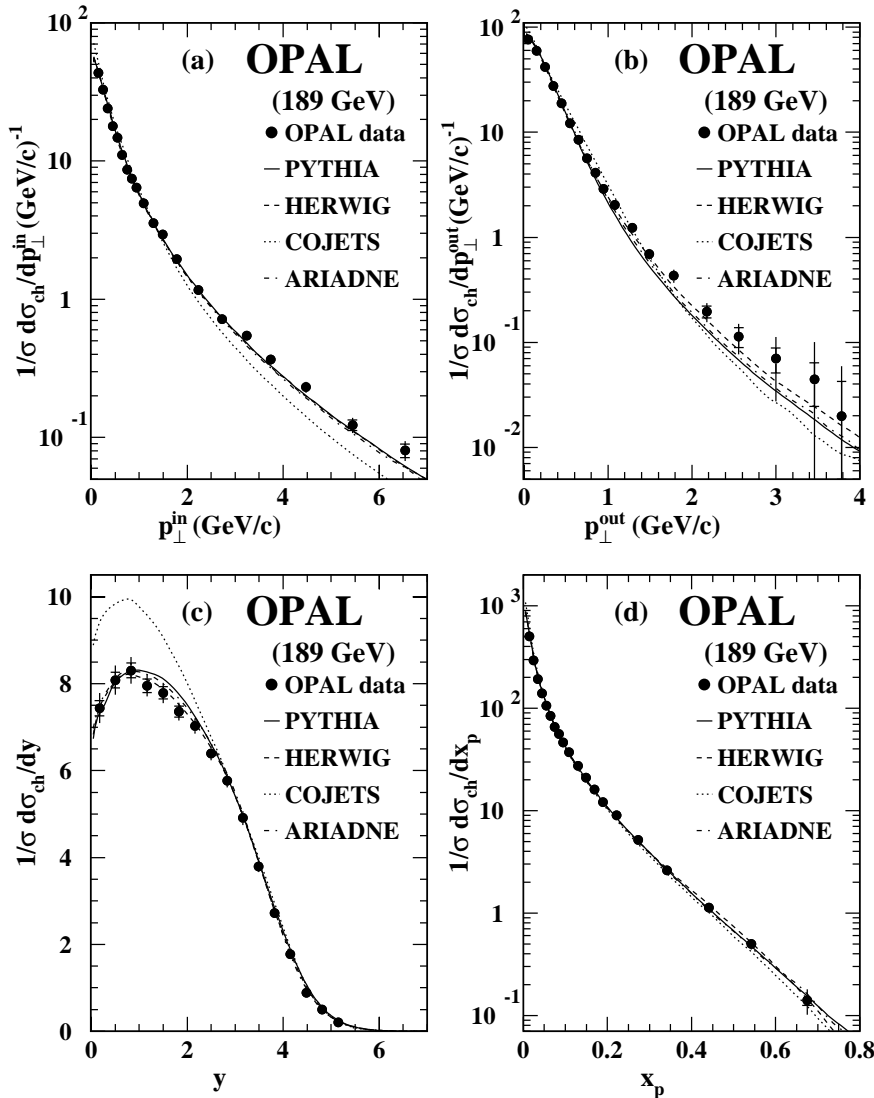
Fig. 11a–d. Distributions of the momenta $p_\perp^{\rm in}$, $p_\perp^{\rm out}$ and of the rapidity, y; **d** shows the fragmentation function $1/\sigma\cdot{\rm d}\sigma_{\rm ch}/{\rm d}x_p$ with $x_p = 2p/\sqrt{s}$; all compared to PYTHIA, HERWIG, COJETS and ARIADNE predictions

corrected using a bin-by-bin multiplication method. The bin-by-bin corrections are typically smaller than 10–15%.

The charged particle multiplicity distribution, corrected for experimental effects using an unfolding matrix, is tabulated in Table 8. The data are shown for our 189 GeV sample in Fig. 10a. The COJETS model, as indicated in the figure, predicts too many high multiplicity events and clearly disagrees with the data. The PYTHIA and ARIADNE models predict mutually indistinguishable distributions which describe the data reasonably well. The HERWIG model gives a somewhat better description for low and intermediate values.

We determine the mean values to be:

$$\langle n_{\rm ch}\rangle(172\ {\rm GeV}) = 25.77 \pm 0.58({\rm stat.}) \pm 0.88({\rm syst.}),$$
$$\langle n_{\rm ch}\rangle(183\ {\rm GeV}) = 26.85 \pm 0.27({\rm stat.}) \pm 0.52({\rm syst.}), \quad (5)$$
$$\langle n_{\rm ch}\rangle(189\ {\rm GeV}) = 26.95 \pm 0.16({\rm stat.}) \pm 0.51({\rm syst.}),$$

The systematic errors are detailed in Table 9. The values of the dispersion D, the ratio $\langle n_{\rm ch}\rangle/D$, the normalised second moment C_2 and the second binomial moment $\mathcal{R}_2$ can be found in Table 8.

As a consistency check, the mean charged multiplicity is also computed by integrating the corrected rapidity distribution, and the fragmentation function, as determined in the next section. Both the rapidity distribution and the fragmentation function give results in good agreement with the one from the direct measurement presented in this section.

Figure 10b shows our measurements of $\langle n_{\rm ch}\rangle$ together with results from OPAL at lower c.m. energies. The data are compared to those of the other LEP experiments and to analytic QCD or Monte Carlo predictions. The predicted value of $\langle n_{\rm ch}\rangle(189\ {\rm GeV})$ from PYTHIA is 27.6. This value changes by up to 0.4 when the hadronization parameters b and σ_Q and the parton virtuality cutoff parameter Q_0 are varied by ± 1 standard deviation about their tuned values [15]. The values from ARIADNE and HERWIG are 27.5 and 27.2 respectively. The measured value is therefore about one standard deviation low compared to the PYTHIA and ARIADNE models. This trend is seen at all c.m. energies of the LEP-2 data. However, this might be only a consequence of the high correlation
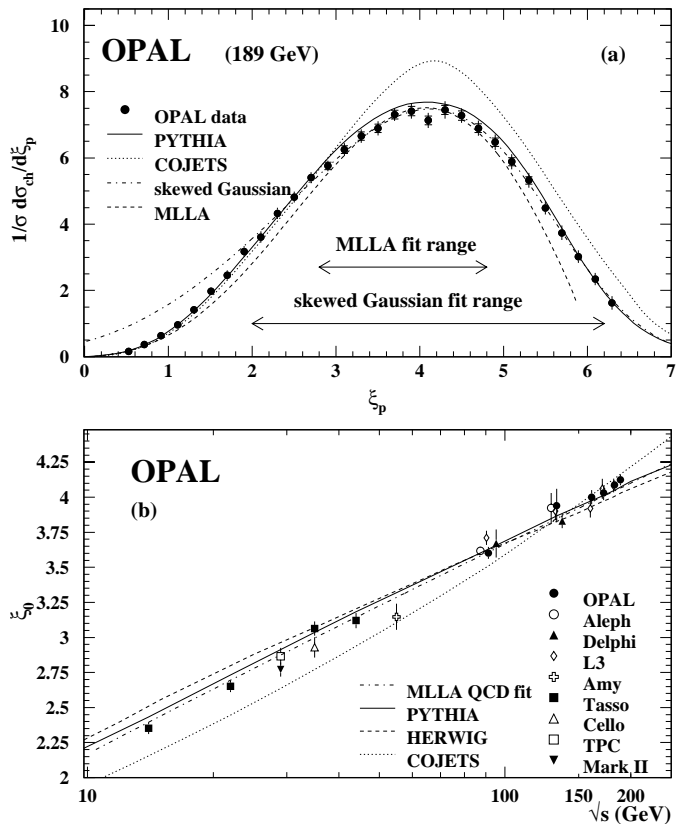
Fig. 12. a Distribution of $\xi_p = \ln(1/x_p)$ for charged particles at $\sqrt{s}=$ 189 GeV. Also shown are a fit of a skewed Gaussian and predictions by MLLA QCD, PYTHIA and COJETS. The curve for the ARIADNE prediction is almost indistinguishable from the PYTHIA prediction and is omitted. **b** Evolution of the position of the peak of the ξ_p distribution, ξ_0, with c.m. energy $\sqrt{s}$, compared with a fit of a MLLA QCD prediction to the previous measurements and with predictions by PYTHIA, HERWIG and COJETS

Fig. 13. Results for the normalisation factor K in the MLLA description of the ξ_p distribution, compared with results from fits to the ξ_p distribution at lower energies [54]

Table 9. Results with statistical and systematic uncertainties for the mean charged multiplicity $\langle n_{\rm ch}\rangle$ at $\sqrt{s} = 172$, 183 and 189 GeV

	$\langle n_{\rm ch}\rangle$		
	172 GeV	183 GeV	189 GeV
standard result	25.77	26.85	26.95
statistical error	0.58	0.27	0.16
Alternative $\sqrt{s'}$	-0.15	$+0.01$	-0.01
Background $\pm 5\%$	$+0.01$	$+0.02$	-0.02
$|d_0| < 5$ cm	$+0.29$	$+0.05$	$+0.05$
$|z_0| < 10$ cm	$+0.33$	$+0.35$	$+0.34$
$N_{hits} > 80$	-0.07	-0.08	-0.08
$|\cos\theta_T| < 0.7$	-0.05	$+0.12$	$+0.20$
HERWIG	<0.01	-0.35	-0.20
W_{QCD}	$+0.74$	-0.05	$+0.23$
Tot. syst. error	0.88	0.52	0.51

between the systematic uncertainties of the OPAL measurements. COJETS predicts the charged multiplicity to be above 30, well above the measured value. The models have been tuned to agree with the OPAL data taken at the Z^0 peak with $\langle n_{\rm ch}\rangle(M_{Z^0}) = 21.05\pm0.01({\rm stat.})\pm0.20({\rm syst.})$ [48].

The dispersion D of the data, $D(189\ {\rm GeV}) = 8.45 \pm 0.12({\rm stat.})\pm0.34({\rm syst.})$ is better described by the PYTHIA and ARIADNE Monte Carlo samples, which predict 8.65 and 8.58 respectively. In contrast, the HERWIG model predicts $D(189\ {\rm GeV}) = 9.25$, more than two standard deviations too large.

The dash-dotted curve in Fig. 10b shows the NLLA QCD prediction [49] for the energy evolution of the charged particle multiplicity, with parameters fitted to all available data points between 12 and 161 GeV [1,50,3,4,7,6,48]. The NLLA calculation predicts a mean charged multiplicity at 189 GeV of 27.6. Variations in the quark flavour composition at the different c.m. energies do not significantly influence the results of the fit.
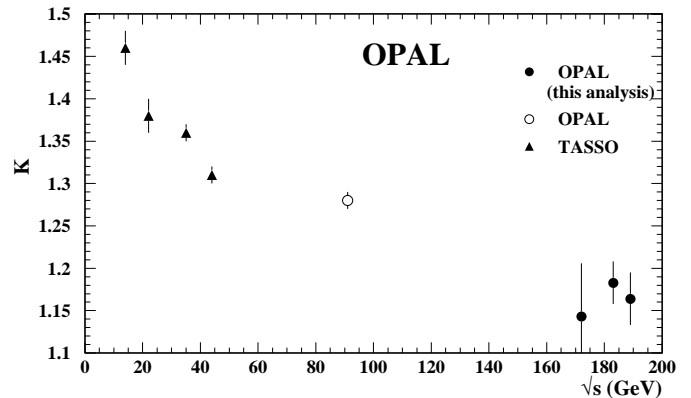
5.4 Charged particle momentum spectra

We measure the charged particle fragmentation function, $1/\sigma \cdot {\rm d}\sigma_{\rm ch}/{\rm d}x_p$, and the ξ_p distribution, $1/\sigma \cdot {\rm d}\sigma_{\rm ch}/{\rm d}\xi_p$, where $x_p = 2p/\sqrt{s}$, $\xi_p = \ln(1/x_p)$ and p is the measured track momentum, using the same methods as in our previous publications [1,2]. We determine the rapidity distribution, $y = |\ln(\frac{E+p_\parallel}{E-p_\parallel})|$, where $p_\parallel$ is the momentum component parallel to the thrust axis and E is the energy of the particle. We also study the distribution of the 3-momentum components parallel, $p_\perp^{\rm in}$, and perpendicular, $p_\perp^{\rm out}$, to the event plane. This plane is defined by the eigenvectors of the momentum tensor associated with the two largest eigenvalues, as in [1].

The $p_\perp^{\rm in}$, $p_\perp^{\rm out}$ and y distributions for events with a c.m. energy of $\sqrt{s} = 189$ GeV are shown in Fig. 11 and are tabulated in Tables 10, 11 and 12. We observe good agreement between PYTHIA, HERWIG and ARIADNE and the data for the $p_\perp^{\rm in}$ distributions. However, the slopes of

Table 10. Measured values for the momentum spectra $R(p_\perp^{in}) = 1/\sigma \cdot d\sigma_{ch}/dp_\perp^{in}$ in the event plane at $\sqrt{s} = 172$, 183 and 189 GeV. The first error is statistical, the second systematic. The mean values are also shown

$p_\perp^{in}$	$R(p_\perp^{in})$ (172 GeV)		$R(p_\perp^{in})$ (183 GeV)		$R(p_\perp^{in})$ (189 GeV)	
0.0-0.1	52.3 ± 2.2	± 2.1	55.4 ± 1.0	± 1.9	53.7 ± 0.6	± 1.7
0.1-0.2	39.8 ± 1.6	± 1.7	42.4 ± 0.8	± 1.3	43.4 ± 0.5	± 1.2
0.2-0.3	31.2 ± 1.3	± 1.1	32.1 ± 0.7	± 0.9	32.7 ± 0.4	± 0.7
0.3-0.4	23.9 ± 1.1	± 1.0	24.2 ± 0.6	± 0.6	24.1 ± 0.3	± 0.4
0.4-0.5	18.6 ± 1.1	± 0.7	19.1 ± 0.5	± 0.5	17.9 ± 0.3	± 0.3
0.5-0.6	16.3 ± 1.0	± 0.6	13.7 ± 0.4	± 0.4	14.8 ± 0.3	± 0.3
0.6-0.7	10.9 ± 0.9	± 0.4	11.4 ± 0.4	± 0.3	11.1 ± 0.2	± 0.2
0.7-0.8	8.43 ± 0.70	± 0.37	9.40 ± 0.36	± 0.21	8.65 ± 0.20	± 0.17
0.8-0.9	7.62 ± 0.74	± 0.40	7.09 ± 0.31	± 0.18	7.46 ± 0.19	± 0.13
0.9-1.0	5.67 ± 0.60	± 0.38	5.92 ± 0.30	± 0.22	6.42 ± 0.18	± 0.19
1.0-1.2	3.88 ± 0.39	± 0.40	4.52 ± 0.19	± 0.23	4.95 ± 0.12	± 0.16
1.2-1.4	2.82 ± 0.35	± 0.39	3.95 ± 0.19	± 0.25	3.56 ± 0.10	± 0.13
1.4-1.6	2.28 ± 0.31	± 0.31	2.65 ± 0.15	± 0.17	2.94 ± 0.09	± 0.08
1.6-2.0	1.78 ± 0.22	± 0.19	1.89 ± 0.10	± 0.12	1.95 ± 0.06	± 0.06
2.0-2.5	1.00 ± 0.14	± 0.11	1.10 ± 0.07	± 0.06	1.16 ± 0.04	± 0.05
2.5-3.0	0.47 ± 0.09	± 0.06	0.75 ± 0.06	± 0.05	0.72 ± 0.03	± 0.03
3.0-3.5	0.38 ± 0.09	± 0.07	0.49 ± 0.04	± 0.05	0.55 ± 0.03	± 0.03
3.5-4.0	0.27 ± 0.08	± 0.06	0.29 ± 0.04	± 0.03	0.37 ± 0.02	± 0.02
4.0-5.0	0.17 ± 0.04	± 0.05	0.22 ± 0.02	± 0.03	0.23 ± 0.01	± 0.02
5.0-6.0	0.06 ± 0.03	± 0.02	0.13 ± 0.02	± 0.02	0.12 ± 0.01	± 0.01
6.0-7.0	0.07 ± 0.03	± 0.03	0.05 ± 0.01	± 0.02	0.08 ± 0.01	± 0.01
7.0-8.0	0.06 ± 0.03	± 0.03	0.02 ± 0.01	± 0.01	0.04 ± 0.01	± 0.01
$\langle p_\perp^{in} \rangle$	$0.593 \pm 0.018 \pm 0.016$		$0.622 \pm 0.008 \pm 0.009$		$0.647 \pm 0.005 \pm 0.011$	

the $p_\perp^{in}$ distributions of the COJETS prediction are somewhat steeper than the data. In case of the $p_\perp^{out}$ distribution, not only COJETS but to lesser extent also PYTHIA, HERWIG and ARIADNE predict a slightly softer $p_\perp^{out}$ spectrum than the spectrum observed in the data. In the y distribution, there is reasonable agreement of the PYTHIA, HERWIG and ARIADNE Monte Carlo models with the data. The COJETS Monte Carlo model significantly overestimates the production of charged particles with low values of y.

The fragmentation function and the ξ_p distribution are shown in Figs. 11 d and 12 a together with the Monte Carlo predictions. Numerical values of these data are given in Tables 13 and 14. The spectrum of charged particles with large momentum fraction x_p is well described by all Monte Carlo models. The shape of the ξ_p distribution is well described by PYTHIA, although their normalisation is somewhat higher, reflecting the difference between the predicted and the observed charged particle multiplicity (see Sect. 5.3). The COJETS Monte Carlo predicts too many particles in the region of the peak and at large values of ξ_p, where low momentum particles contribute. In the LLA approach, this is the region where soft gluon production is reduced as a consequence of destructive interference.

Based on the concept of local parton hadron duality (LPHD)[51] within the leading-log approximation of QCD calculations (LLA)[52] one expects a Gaussian shape of the ξ_p distribution. The peak of the distribution is predicted to have an almost logarithmic variation with energy. The next to leading-log approximation of QCD calculations[51,53] predicts the shape to be a Gaussian with higher moments (skewed Gaussian), and the same energy dependence of the peak as the LLA. We fit a skewed Gaussian of the form suggested in [53] to the region $2.0 < \xi_p < 6.2$ of the three ξ_p distributions and determine the positions of the peaks, ξ_0, to be

$$\xi_0(172\text{ GeV}) = 4.031 \pm 0.033(\text{stat.}) \pm 0.041(\text{syst.}),$$
$$\xi_0(183\text{ GeV}) = 4.087 \pm 0.014(\text{stat.}) \pm 0.030(\text{syst.}), \quad (6)$$
$$\xi_0(189\text{ GeV}) = 4.124 \pm 0.010(\text{stat.}) \pm 0.037(\text{syst.}).$$

The systematic uncertainty takes into account experimental effects as described in Sect. 4.3 and the uncertainty due to the choice of the fit range. The fit range was reduced to $3.2 < \xi_p < 4.8$ and increased to $1.6 < \xi_p < 6.6$. The larger deviation from the result with the standard fit range was taken as systematic uncertainty and added in quadrature to the other effects. All systematic effects are summarised in Table 15.

Table 11. Measured values for the momentum spectra $R(p_\perp^{\text{out}}) = 1/\sigma \cdot \mathrm{d}\sigma_{\text{ch}}/\mathrm{d}p_\perp^{\text{out}}$ out of the event plane at $\sqrt{s} = 172$, 183 and 189 GeV. The first error is statistical, the second systematic. The mean values are also shown

$p_\perp^{\text{out}}$	$R(p_\perp^{\text{out}})$ (172 GeV)		$R(p_\perp^{\text{out}})$ (183 GeV)		$R(p_\perp^{\text{out}})$ (189 GeV)	
0.0-0.1	71.5 ± 2.3	± 2.3	77.2 ± 1.2	± 1.7	76.2 ± 0.7	± 1.6
0.1-0.2	59.1 ± 2.0	± 1.7	59.1 ± 1.0	± 1.1	59.8 ± 0.6	± 1.1
0.2-0.3	39.7 ± 1.6	± 1.1	41.1 ± 0.7	± 0.6	41.7 ± 0.5	± 0.7
0.3-0.4	26.2 ± 1.3	± 0.9	27.9 ± 0.6	± 0.5	27.6 ± 0.4	± 0.4
0.4-0.5	18.4 ± 1.2	± 0.7	19.0 ± 0.5	± 0.5	18.8 ± 0.3	± 0.4
0.5-0.6	11.8 ± 1.0	± 0.5	11.6 ± 0.4	± 0.3	12.2 ± 0.3	± 0.3
0.6-0.7	7.63 ± 0.75	± 0.51	8.29 ± 0.36	± 0.29	8.45 ± 0.22	± 0.27
0.7-0.8	3.94 ± 0.57	± 0.41	5.30 ± 0.29	± 0.19	5.65 ± 0.18	± 0.19
0.8-0.9	3.56 ± 0.49	± 0.59	4.15 ± 0.27	± 0.25	4.11 ± 0.16	± 0.13
0.9-1.0	2.46 ± 0.45	± 0.49	2.82 ± 0.22	± 0.20	2.91 ± 0.13	± 0.10
1.0-1.2	1.76 ± 0.31	± 0.36	1.96 ± 0.15	± 0.16	2.04 ± 0.09	± 0.09
1.2-1.4	0.97 ± 0.20	± 0.18	1.25 ± 0.12	± 0.19	1.23 ± 0.07	± 0.08
1.4-1.6	0.62 ± 0.18	± 0.13	0.62 ± 0.09	± 0.13	0.69 ± 0.05	± 0.06
1.6-2.0	0.33 ± 0.11	± 0.90	0.40 ± 0.05	± 0.13	0.43 ± 0.04	± 0.05
2.0-2.4	0.01 ± 0.04	± 0.03	0.16 ± 0.04	± 0.06	0.20 ± 0.03	± 0.03
2.4-2.8	0.04 ± 0.05	± 0.15	0.04 ± 0.03	± 0.03	0.11 ± 0.02	± 0.03
2.8-3.2	–		0.04 ± 0.03	± 0.10	0.07 ± 0.02	± 0.04
3.2-3.6	–		0.01 ± 0.02	± 0.01	0.04 ± 0.02	± 0.05
3.6-4.0	–		–		0.02 ± 0.02	± 0.03
$\langle p_\perp^{\text{out}} \rangle$	0.282 ± 0.007 ± 0.022		0.289 ± 0.003 ± 0.008		0.300 ± 0.003 ± 0.004	

Table 12. Measured values for the rapidity $R(y) = 1/\sigma \cdot \mathrm{d}\sigma_{\text{ch}}/\mathrm{d}y$ distributions at $\sqrt{s} = 172$, 183 and 189 GeV. The first error is statistical, the second systematic. The mean values are also shown

y	$R(y)$ (172 GeV)		$R(y)$ (183 GeV)		$R(y)$ (189 GeV)	
0.00-0.33	7.56 ± 0.60	± 0.51	7.40 ± 0.29	± 0.35	7.44 ± 0.18	± 0.30
0.33-0.67	6.86 ± 0.60	± 0.41	7.45 ± 0.29	± 0.32	8.08 ± 0.18	± 0.29
0.67-1.00	6.99 ± 0.57	± 0.44	7.60 ± 0.28	± 0.26	8.31 ± 0.17	± 0.25
1.00-1.33	6.98 ± 0.49	± 0.35	7.51 ± 0.25	± 0.23	7.95 ± 0.15	± 0.19
1.33-1.67	6.47 ± 0.47	± 0.30	8.07 ± 0.24	± 0.22	7.79 ± 0.14	± 0.19
1.67-2.00	7.74 ± 0.43	± 0.34	7.30 ± 0.21	± 0.19	7.36 ± 0.12	± 0.16
2.00-2.33	6.72 ± 0.41	± 0.28	6.99 ± 0.19	± 0.21	7.02 ± 0.11	± 0.14
2.33-2.67	6.40 ± 0.36	± 0.27	6.45 ± 0.17	± 0.18	6.40 ± 0.10	± 0.12
2.67-3.00	5.85 ± 0.34	± 0.24	5.89 ± 0.15	± 0.16	5.77 ± 0.09	± 0.13
3.00-3.33	4.45 ± 0.28	± 0.20	4.96 ± 0.14	± 0.13	4.91 ± 0.08	± 0.14
3.33-3.67	4.37 ± 0.32	± 0.20	4.00 ± 0.13	± 0.13	3.80 ± 0.07	± 0.11
3.67-4.00	2.38 ± 0.21	± 0.11	2.97 ± 0.11	± 0.12	2.72 ± 0.06	± 0.08
4.00-4.33	1.62 ± 0.16	± 0.11	1.76 ± 0.09	± 0.08	1.77 ± 0.05	± 0.07
4.33-4.67	1.19 ± 0.15	± 0.12	1.00 ± 0.06	± 0.07	0.89 ± 0.03	± 0.07
4.67-5.00	0.31 ± 0.08	± 0.05	0.51 ± 0.05	± 0.05	0.50 ± 0.03	± 0.05
5.00-5.33	0.19 ± 0.06	± 0.06	0.22 ± 0.03	± 0.03	0.21 ± 0.02	± 0.02
5.33-5.67	0.045 ± 0.026 ± 0.028		0.089 ± 0.017 ± 0.015		0.082 ± 0.010 ± 0.010	
5.67-6.00	0.019 ± 0.019 ± 0.017		0.039 ± 0.011 ± 0.009		0.031 ± 0.006 ± 0.006	
6.00-6.33	0.012 ± 0.012 ± 0.013		0.007 ± 0.004 ± 0.001		0.007 ± 0.003 ± 0.002	
$\langle y \rangle$	1.877 ± 0.024 ± 0.032		1.877 ± 0.011 ± 0.026		1.837 ± 0.006 ± 0.018	

Table 13. Measured values for the fragmentation functions $R(x_p) = 1/\sigma \cdot d\sigma_{ch}/dx_p$ at $\sqrt{s} = 172$, 183 and 189 GeV. The first error is statistical, the second systematic. The mean values are also shown

x_p	$R(x_p)$ (172 GeV)		$R(x_p)$ (183 GeV)		$R(x_p)$ (189 GeV)	
0.00-0.01	749. ± 30.	± 30.	812. ± 15.	± 21.	855. ± 9.	± 20.
0.01-0.02	472. ± 20.	± 22.	515. ± 10.	± 13.	506. ± 6.	± 10.
0.02-0.03	281. ± 15.	± 11.	295. ± 7.	± 7.	295. ± 4.	± 7.
0.03-0.04	194. ± 12.	± 8.	191. ± 5.	± 6.	192. ± 3.	± 4.
0.04-0.05	130. ± 10.	± 6.	147. ± 4.	± 4.	140. ± 3.	± 3.
0.05-0.06	117. ± 8.	± 7.	103. ± 4.	± 3.	106. ± 2.	± 2.
0.06-0.07	77.4 ± 7.3	± 4.3	87.9 ± 3.4	± 2.3	84.4 ± 2.0	± 2.6
0.07-0.08	66.8 ± 6.0	± 4.0	64.3 ± 2.9	± 1.6	66.2 ± 1.7	± 2.0
0.08-0.09	50.8 ± 5.4	± 3.4	55.1 ± 2.6	± 1.6	56.0 ± 1.6	± 1.9
0.09-0.10	42.9 ± 4.9	± 3.2	46.2 ± 2.3	± 1.4	46.4 ± 1.4	± 1.2
0.10-0.12	38.4 ± 3.6	± 2.8	35.2 ± 1.5	± 1.3	37.0 ± 0.9	± 1.3
0.12-0.14	26.5 ± 3.1	± 1.5	30.1 ± 1.4	± 1.0	27.3 ± 0.8	± 1.4
0.14-0.16	25.9 ± 2.5	± 1.5	22.7 ± 1.2	± 1.1	21.1 ± 0.7	± 1.1
0.16-0.18	20.0 ± 2.5	± 1.3	18.9 ± 1.1	± 1.3	16.0 ± 0.6	± 0.9
0.18-0.20	14.7 ± 2.0	± 1.1	11.7 ± 0.9	± 0.9	12.1 ± 0.5	± 0.6
0.20-0.25	8.54 ± 0.93	± 1.11	9.66 ± 0.50	± 0.67	9.03 ± 0.28	± 0.38
0.25-0.30	3.92 ± 0.70	± 0.55	5.53 ± 0.37	± 0.38	5.20 ± 0.21	± 0.22
0.30-0.40	2.69 ± 0.34	± 0.37	2.65 ± 0.18	± 0.16	2.60 ± 0.10	± 0.10
0.40-0.50	1.09 ± 0.24	± 0.14	1.34 ± 0.12	± 0.14	1.13 ± 0.07	± 0.06
0.50-0.60	0.77 ± 0.18	± 0.12	0.51 ± 0.08	± 0.08	0.50 ± 0.04	± 0.04
0.60-0.80	0.16 ± 0.06	± 0.06	0.12 ± 0.02	± 0.04	0.14 ± 0.02	± 0.04
$\langle x_p \rangle$	0.0495 ± 0.0011 ± 0.0010		0.0480 ± 0.0005 ± 0.0007		0.0464 ± 0.0003 ± 0.0007	

In Fig. 12b we show our measurements of ξ_0 together with measurements taken at various c.m. energies [2,1, 3,5,8,54,55], and the PYTHIA, HERWIG and COJETS predictions. The dash-dotted curve shows the prediction for the energy evolution by the modified leading-log approximation (MLLA) [56] with parameters fitted to the different energies, excluding the results of this paper. The values of the MLLA prediction extrapolated to $\sqrt{s} = 172$, 183 and 189 GeV of 4.01±0.01, 4.05±0.01 and 4.07±0.01 are lower than our measurements. As noted in our previous publications [1,2], the fit is dominated by contributions from the data points with small errors at 29 and 35 GeV. The PYTHIA and HERWIG predictions are very similar to the MLLA fit, while the COJETS prediction does not agree with the data.

In Fig. 12a also the shape predicted by MLLA [57] is shown. The MLLA prediction is determined by two parameters, an effective QCD scale Λ_{eff} and a normalisation factor $K(\sqrt{s})$ which within the framework of LPHD is expected to have a weak c.m. energy dependence. We fix Λ_{eff} to the value determined in [54], $\Lambda_{eff} = 0.253$, and fit the formula to the measured charged particle momentum spectra in the region $2.8 < \xi_p < 4.8$. The result of this fit to the $\sqrt{s} = 189$ GeV data is shown in Fig. 12 **a**. The MLLA description and data show good agreement in the peak region but disagree at large ξ_p where kinematic

effects become important and the perturbative QCD calculations are not valid [58]. The values obtained for the normalisation factor K are:

$$K(\sqrt{s} = 172 \text{ GeV}) = 1.143 \pm 0.030(\text{stat.})$$
$$\pm 0.056(\text{syst.}),$$
$$K(\sqrt{s} = 183 \text{ GeV}) = 1.183 \pm 0.010(\text{stat.})$$
$$\pm 0.023(\text{syst.}),$$
$$K(\sqrt{s} = 189 \text{ GeV}) = 1.164 \pm 0.008(\text{stat.})$$
$$\pm 0.030(\text{syst.}). \qquad (7)$$

To estimate the uncertainty due to the choice of the fit range, the fit range was reduced to $3.6 < \xi_p < 4.2$ and increased to $2.4 < \xi_p < 5.2$. the systematic uncertainty is shown in Table 16. In Fig. 13, these numbers are compared with results for the normalisation factors obtained in [54] for ξ_p distributions at lower c.m. energies. The values from the new measurements are significantly below the value at $\sqrt{s} = M_{Z^0}$, $K(M_{Z^0}) = 1.28 \pm 0.01$, thus following the observed trend of decreasing values for K with increasing c.m. energy. A decrease of K values might be caused by higher order effects as discussed in [59].

MLLA makes several predictions for relations between the different quantities that can be used to describe the centre of the ξ_p distribution, i.e. the position of the max-

Table 14. Measured values for the $R(\xi_p) = 1/\sigma \cdot \mathrm{d}\sigma_{\mathrm{ch}}/\mathrm{d}\xi_p$ distributions at $\sqrt{s} = 172$, 183 and 189 GeV. The first error is statistical, the second systematic

ξ_p	$R(\xi_p)$ (172 GeV)	$R(\xi_p)$ (183 GeV)	$R(\xi_p)$ (189 GeV)
0.0-0.2	$0.005 \pm 0.006 \pm 0.003$	$0.015 \pm 0.005 \pm 0.005$	$0.015 \pm 0.003 \pm 0.005$
0.2-0.4	$0.05 \pm 0.03\ \pm 0.02$	$0.07 \pm 0.02\ \pm 0.02$	$0.08 \pm 0.01\ \pm 0.02$
0.4-0.6	$0.30 \pm 0.08\ \pm 0.06$	$0.11 \pm 0.03\ \pm 0.02$	$0.16 \pm 0.02\ \pm 0.02$
0.6-0.8	$0.42 \pm 0.10\ \pm 0.06$	$0.46 \pm 0.05\ \pm 0.09$	$0.36 \pm 0.03\ \pm 0.04$
0.8-1.0	$0.57 \pm 0.12\ \pm 0.07$	$0.65 \pm 0.06\ \pm 0.06$	$0.63 \pm 0.03\ \pm 0.05$
1.0-1.2	$1.01 \pm 0.15\ \pm 0.14$	$1.00 \pm 0.08\ \pm 0.08$	$0.96 \pm 0.04\ \pm 0.05$
1.2-1.4	$1.12 \pm 0.19\ \pm 0.14$	$1.54 \pm 0.09\ \pm 0.10$	$1.42 \pm 0.05\ \pm 0.06$
1.4-1.6	$1.90 \pm 0.22\ \pm 0.24$	$2.07 \pm 0.12\ \pm 0.15$	$1.98 \pm 0.06\ \pm 0.08$
1.6-1.8	$2.86 \pm 0.31\ \pm 0.20$	$2.74 \pm 0.13\ \pm 0.15$	$2.46 \pm 0.07\ \pm 0.12$
1.8-2.0	$3.90 \pm 0.31\ \pm 0.19$	$3.36 \pm 0.14\ \pm 0.16$	$3.18 \pm 0.08\ \pm 0.13$
2.0-2.2	$3.62 \pm 0.33\ \pm 0.20$	$3.78 \pm 0.16\ \pm 0.13$	$3.61 \pm 0.09\ \pm 0.15$
2.2-2.4	$4.18 \pm 0.36\ \pm 0.24$	$4.19 \pm 0.16\ \pm 0.14$	$4.33 \pm 0.10\ \pm 0.14$
2.4-2.6	$4.62 \pm 0.37\ \pm 0.28$	$4.90 \pm 0.18\ \pm 0.16$	$4.82 \pm 0.10\ \pm 0.13$
2.6-2.8	$5.06 \pm 0.42\ \pm 0.26$	$5.27 \pm 0.19\ \pm 0.14$	$5.40 \pm 0.11\ \pm 0.13$
2.8-3.0	$6.17 \pm 0.41\ \pm 0.32$	$5.66 \pm 0.19\ \pm 0.19$	$5.76 \pm 0.11\ \pm 0.11$
3.0-3.2	$5.98 \pm 0.47\ \pm 0.24$	$6.59 \pm 0.20\ \pm 0.19$	$6.25 \pm 0.12\ \pm 0.15$
3.2-3.4	$5.93 \pm 0.43\ \pm 0.23$	$6.42 \pm 0.21\ \pm 0.23$	$6.66 \pm 0.12\ \pm 0.16$
3.4-3.6	$8.06 \pm 0.52\ \pm 0.36$	$6.93 \pm 0.22\ \pm 0.22$	$6.89 \pm 0.13\ \pm 0.17$
3.6-3.8	$6.88 \pm 0.48\ \pm 0.44$	$7.46 \pm 0.23\ \pm 0.23$	$7.31 \pm 0.13\ \pm 0.14$
3.8-4.0	$6.30 \pm 0.48\ \pm 0.42$	$7.67 \pm 0.24\ \pm 0.21$	$7.41 \pm 0.14\ \pm 0.18$
4.0-4.2	$7.30 \pm 0.50\ \pm 0.51$	$7.51 \pm 0.22\ \pm 0.24$	$7.13 \pm 0.13\ \pm 0.19$
4.2-4.4	$6.33 \pm 0.44\ \pm 0.37$	$7.61 \pm 0.24\ \pm 0.27$	$7.45 \pm 0.14\ \pm 0.22$
4.4-4.6	$6.93 \pm 0.45\ \pm 0.41$	$6.99 \pm 0.22\ \pm 0.22$	$7.28 \pm 0.14\ \pm 0.17$
4.6-4.8	$6.56 \pm 0.46\ \pm 0.45$	$6.71 \pm 0.21\ \pm 0.17$	$6.90 \pm 0.13\ \pm 0.18$
4.8-5.0	$6.39 \pm 0.48\ \pm 0.44$	$6.25 \pm 0.20\ \pm 0.18$	$6.48 \pm 0.13\ \pm 0.20$
5.0-5.2	$5.18 \pm 0.41\ \pm 0.42$	$5.92 \pm 0.20\ \pm 0.24$	$5.89 \pm 0.12\ \pm 0.20$
5.2-5.4	$4.40 \pm 0.38\ \pm 0.37$	$4.95 \pm 0.19\ \pm 0.21$	$5.32 \pm 0.11\ \pm 0.19$
5.4-5.6	$3.95 \pm 0.38\ \pm 0.40$	$4.11 \pm 0.17\ \pm 0.22$	$4.49 \pm 0.10\ \pm 0.17$
5.6-5.8	$2.85 \pm 0.29\ \pm 0.24$	$3.63 \pm 0.16\ \pm 0.20$	$3.74 \pm 0.09\ \pm 0.20$
5.8-6.0	$2.58 \pm 0.30\ \pm 0.29$	$2.59 \pm 0.14\ \pm 0.20$	$3.02 \pm 0.09\ \pm 0.17$
6.0-6.2	$2.12 \pm 0.29\ \pm 0.29$	$2.17 \pm 0.13\ \pm 0.17$	$2.34 \pm 0.08\ \pm 0.17$
6.2-6.4	$0.92 \pm 0.29\ \pm 0.43$	$1.47 \pm 0.14\ \pm 0.28$	$1.62 \pm 0.08\ \pm 0.19$

imum ξ_0, the mean value $\langle \xi_p \rangle$ and the median value ξ_m which is defined as the value where $\int_0^{\xi_m}(\mathrm{d}\sigma_{\mathrm{ch}}/\mathrm{d}\xi_p)\mathrm{d}\xi_p$ is equal to $\int_{\xi_m}^{\infty}(\mathrm{d}\sigma_{\mathrm{ch}}/\mathrm{d}\xi_p)\mathrm{d}\xi_p$. The difference $\xi_0 - \langle \xi_p \rangle$ is predicted to be approximately 0.351 (0.355) for 3(5) active flavours, independent from the c.m. energy[57]. The first non-leading corrections to this value cannot be predicted at the moment. However, this correction has been taken into account for the calculation of the ratio of differences, $(\xi_0 - \langle \xi_p \rangle)/(\xi_m - \langle \xi_p \rangle)$ which is predicted to be 3.5 (3.4) for 3(5) active flavours for the c.m energies considered in this paper and assuming $\Lambda_{eff} = 0.253$. In our analysis, we measure

$$\xi_0 - \langle \xi_p \rangle (172\text{ GeV}) = \quad 0.054 \pm 0.023 (\text{stat.})$$
$$\pm 0.063 (\text{syst.}),$$

$$\xi_0 - \langle \xi_p \rangle (183\text{ GeV}) = \quad 0.012 \pm 0.010 (\text{stat.})$$
$$\pm 0.064 (\text{syst.}), \qquad (8)$$
$$\xi_0 - \langle \xi_p \rangle (189\text{ GeV}) = -0.035 \pm 0.007 (\text{stat.})$$
$$\pm 0.075 (\text{syst.})$$

and

$$(\xi_0 - \langle \xi_p \rangle)/(\xi_m - \langle \xi_p \rangle)(172\text{ GeV}) = -0.38 \pm 0.56 (\text{stat.})$$
$$\pm 0.42 (\text{syst.}),$$
$$(\xi_0 - \langle \xi_p \rangle)/(\xi_m - \langle \xi_p \rangle)(183\text{ GeV}) = -0.06 \pm 0.44 (\text{stat.})$$
$$\pm 0.27 (\text{syst.}), \qquad (9)$$
$$(\xi_0 - \langle \xi_p \rangle)/(\xi_m - \langle \xi_p \rangle)(189\text{ GeV}) = \quad 0.16 \pm 0.33 (\text{stat.})$$
$$\pm 0.22 (\text{syst.}).$$

Table 15. Results with statistical and systematic uncertainties for the position ξ_0 of the peak of the ξ_p distribution at $\sqrt{s} = 172$, 183 and 189 GeV

	ξ_0		
	172 GeV	183 GeV	189 GeV
standard result	4.031	4.087	4.124
statistical error	0.033	0.014	0.010
Alternative $\sqrt{s'}$	0.012	<0.001	0.010
Background ± 5 %	−0.002	−0.002	0.002
$|d_0| < 5$ cm	−0.006	0.011	<0.001
$|z_0| < 10$ cm	−0.006	−0.006	−0.005
$N_{hits} > 80$	−0.026	−0.023	−0.024
$|\cos\theta_T| < 0.7$	0.012	−0.002	0.002
HERWIG	0.005	0.013	0.006
W_{QCD}	0.001	−0.001	−0.004
fit range	0.024	0.007	0.025
Tot. syst. error	0.041	0.030	0.037

Table 16. Results for the normalisation factor K in the MLLA description of the ξ_p distribution with statistical and systematic uncertainties at $\sqrt{s} = 172$, 183 and 189 GeV

	K		
	172 GeV	183 GeV	189 GeV
standard result	1.143	1.183	1.164
statistical error	0.030	0.010	0.008
Alternative $\sqrt{s'}$	0.014	−0.001	<0.001
Background ± 5 %	−0.001	0.001	−0.001
$|d_0| < 5$ cm	−0.013	−0.002	<0.001
$|z_0| < 10$ cm	−0.012	−0.012	−0.012
$N_{hits} > 80$	−0.001	<0.001	<0.001
$|\cos\theta_T| < 0.7$	−0.009	−0.006	−0.005
HERWIG	0.012	0.011	0.005
W_{QCD}	0.005	−0.003	−0.007
fit range	0.049	0.015	0.026
Tot. syst. error	0.056	0.023	0.030

Table 17. Results with statistical and systematic uncertainties for the difference of the position ξ_0 of the peak of the ξ_p distribution and its mean value $\langle\xi_p\rangle$ at $\sqrt{s} = 172$, 183 and 189 GeV

	$\xi_0 - \langle\xi_p\rangle$		
	172 GeV	183 GeV	189 GeV
standard result	0.054	0.012	−0.035
statistical error	0.023	0.010	0.007
Alternative $\sqrt{s'}$	0.005	−0.001	0.008
Background ± 5 %	0.001	0.002	−0.003
$|d_0| < 5$ cm	0.003	0.001	0.004
$|z_0| < 10$ cm	−0.002	−0.002	−0.003
$N_{hits} > 80$	−0.015	−0.015	−0.018
$|\cos\theta_T| < 0.7$	−0.017	0.002	0.006
HERWIG	−0.046	−0.059	−0.069
W_{QCD}	0.016	0.005	−0.009
fit range	0.032	0.020	0.020
Tot. syst. error	0.063	0.064	0.075

Table 18. Results with statistical and systematic uncertainties for the ratio of the difference of the position ξ_0 of the peak of the ξ_p distribution and its mean value $\langle\xi_p\rangle$ and the difference between the median and the mean of the ξ_p distribution, $(\xi_0 - \langle\xi_p\rangle)/(\xi_m - \langle\xi_p\rangle)$ at $\sqrt{s} = 172$, 183 and 189 GeV

	$\dfrac{\xi_0 - \langle\xi_p\rangle}{\xi_m - \langle\xi_p\rangle}$		
	172 GeV	183 GeV	189 GeV
standard result	−0.38	−0.06	0.16
statistical error	0.56	0.44	0.33
Alternative $\sqrt{s'}$	−0.05	0.01	−0.03
Background ± 5 %	<0.01	−0.01	0.01
$|d_0| < 5$ cm	−0.03	−0.01	−0.02
$|z_0| < 10$ cm	0.02	0.01	0.01
$N_{hits} > 80$	0.12	0.08	0.07
$|\cos\theta_T| < 0.7$	0.15	−0.01	−0.02
HERWIG	0.34	0.26	0.20
W_{QCD}	−0.14	−0.03	0.04
fit range	0.03	0.02	0.02
Tot. syst. error	0.42	0.27	0.22

The systematic errors are detailed in Tables 17 and 18. The results strongly depend on the high ξ_p region of the ξ_p spectrum, i.e. on the low momentum region where the selection efficiency for tracks is low and the corrections large. In MLLA mass effects are neglected and the ξ_p distribution vanishes for values above $\xi_p = \log(E/\Lambda_{eff})$. In [60,56], a simple procedure was suggested on how to take these effects into account in the MLLA predictions. Indeed, when we fitted these 'modified' MLLA predictions to the ξ_p distribution at $\sqrt{s} = 189$ GeV, it turned out that the fitted values for ξ_0, ξ_m and $\langle\xi_p\rangle$ became numeri-

cally very close to each other such that the value for the difference $\xi_0 - \langle\xi_p\rangle$ almost vanished, consistent with our measurement. This also indicates that the value and even the sign for the ratio $(\xi_0 - \langle\xi_p\rangle)/(\xi_m - \langle\xi_p\rangle)$ is largely undetermined, and depends strongly on the assumptions made in the correction procedure to the MLLA distribu-

tion. A comparison with the measured values is therefore not conclusive.

6 Summary and conclusions

In this paper we have presented measurements of the properties of hadronic events produced at LEP at centre-of-mass energies between 172 and 189 GeV. The 189 GeV data-set comprises approximately 70% of the total luminosity recorded by the OPAL detector at energies above the Z^0 resonance and provides our most precise results of the LEP-2 programme so far.

We have determined the corrected distributions for event shape observables, for the charged particle multiplicity and for charged particle momentum spectra at centre-of-mass energies of $\sqrt{s}$ =172, 183 and 189 GeV. The predictions of the PYTHIA, HERWIG and ARIADNE Monte Carlo models are found to be in general agreement with the measured distributions. While the COJETS Monte Carlo model describes most event shape distributions well, it overestimates the number of soft charged particles produced as observed in the rapidity and $\xi_p = \ln(1/x_p)$ distributions.

From a fit of $\mathcal{O}(\alpha_s^2)$+NLLA QCD predictions to five event shapes and the differential two jet rate, defined using the Durham jet finder, we have determined the strong coupling parameter $\alpha_s(187 \text{ GeV}) = 0.106 \pm 0.001(\text{stat.}) \pm 0.004(\text{syst.})$ at a luminosity weighted centre-of-mass energy of 186.7 GeV. When this is evolved to the Z^0 peak it is in excellent agreement with our previous measurement at $\sqrt{s} = M_{Z^0}$.

The mean charged particle multiplicity has been determined to be $\langle n_{\text{ch}}\rangle(189 \text{ GeV}) = 26.95 \pm 0.16(\text{stat.}) \pm 0.51(\text{syst.})$, about one standard deviation below the NLLA QCD predictions and the PYTHIA and ARIADNE Monte Carlo predictions.

The ξ_p distribution is not in perfect agreement with QCD MLLA calculations. The position of the peak was measured to be $\xi_0(189 \text{ GeV}) = 4.124 \pm 0.010(\text{stat.}) \pm 0.037(\text{syst.})$. This is approximately one and a half standard deviations larger than the expectation for the energy evolution given by a QCD MLLA extrapolation from the results of lower energy experiments.

Our studies show that most of the features of hadronic events produced in e$^+$e$^-$ collisions at energies above the Z^0 mass are well described by QCD in the form of analytic or Monte Carlo predictions, or both.

References

1. OPAL Coll., G. Alexander et al.: Z. Phys. C 72 (1996) 191
2. OPAL Coll., K. Ackerstaff et al.: Z. Phys. C 75 (1997) 193
3. ALEPH Coll., D. Busculic et al.: Z. Phys. C 73 (1997) 409
4. L3 Coll., M. Acciarri et al.: Phys. Lett. B 371 (1996) 137
5. DELPHI Coll., P. Abreu et al.: Z. Phys. C 73 (1997) 229
6. DELPHI Coll., P. Abreu et al.: Phys. Lett. B 372 (1996) 172
7. L3 Coll., M. Acciarri et al.: Phys. Lett. B 404 (1997) 390
8. L3 Coll., M. Acciarri et al.: Phys. Lett. B 444 (1998) 569
9. DELPHI Coll., P. Abreu et al.: Phys. Lett. B 416 (1998) 233
10. S. Bethke, J.E. Pilcher: Annu. Rev. Nucl. Part. Sci. 42 (1992) 251
11. JADE and OPAL Coll., P.Pfeifenschneider et al.: 'QCD Analyses and Determinations of α_s in e$^+$e$^-$ Annihilations at Energies between 35 and 189 GeV', to be submitted to Eur. Phys. J. C
12. OPAL Coll., K. Ahmet et al.: Nucl. Instrum. Methods A 305 (1991) 275
13. J. Allison et al.: Nucl. Instrum. Methods A 317 (1992) 47
14. T. Sjöstrand: Comput. Phys. Commun. 82 (1994) 74
15. OPAL Coll., G. Alexander et al.: Z. Phys. C 69 (1996) 543
16. G. Marchesini et al.: Comput. Phys. Commun. 67 (1992) 465
17. S. Jadach, MPI-München, MPI-PAE/PTh 6/87 (1987)
18. J. Fujimoto et al.: Comput. Phys. Commun. 100 (1997) 128
19. E. Boudinov et al., '$\gamma\gamma$ Event Generators', hep-ph/9512371, Dec. 1995, and in 'Physics at LEP2', eds. G. Altarelli, T. Sjöstrand and F. Zwirner, CERN 96-01, vol.2 (1996) 187
20. S. Jadach et al., Comput. Phys. Commun. 79 (1994) 503
21. L. Lönnblad: Comput. Phys. Commun. 71 (1992) 15
22. R. Odorico: Comput. Phys. Commun. 24 (1981) 119
23. P. Mazzanti, R. Odorico: Nucl. Phys. B 394 (1993) 267
24. OPAL Coll., K. Ackerstaff et al.: Eur. Phys. J. C 6 (1999) 1
25. OPAL Coll., P. D. Acton et al.: Z. Phys. C 59 (1993) 1
26. OPAL Coll., K. Ackerstaff et al.: Eur. Phys. J. C 2 (1998) 441
27. S. Catani et al.: Phys. Lett. B 269 (1991) 432
28. S. Catani, M.H. Seymour: Phys. Lett. B 378 (1996) 287
29. R.K. Ellis, D.A. Ross, A.E. Terrano: Nucl. Phys. B 178 (1981) 421
30. OPAL Coll., G. Abbiendi et al.: Eur. Phys. J. C 8 (1999) 191
31. S. Brandt et al.: Phys. Lett. 12 (1964) 57
32. E. Fahri: Phys. Rev. Lett. 39 (1977) 1587

33. D. P. Barber et al.: Phys. Rev. Lett. 43 (1979) 830
34. J.D. Bjorken, S.J. Brodsky: Phys. Rev. D 1 (1970) 1416
35. SLAC-LBL Coll., G. Hanson et al.: Phys. Rev. Lett. 35 (1975) 1609
36. S.L. Wu, G. Zobernig: Z. Phys. C 2 (1979) 107
37. G. Parisi: Phys. Lett. B 74 (1978) 65; J.F. Donoghue, F.E. Low, S.Y. Pi: Phys. Rev. D 20 (1979) 2759; R.K Ellis, D.A. Ross, A.E. Terrano: Nucl. Phys. B 178 (1981) 421
38. T. Chandramohan, L. Clavelli: Nucl. Phys. B 184 (1981) 365
39. L. Clavelli, D. Wyler: Phys. Lett. B 103 (1981) 383
40. S. Catani, G. Turnock, B.R. Webber: Phys. Lett. B 295 (1992) 269
41. TASSO Coll., W. Braunschweig et al.: Z. Phys. C 47 (1990) 187; AMY Coll., Y. Li et al.: Phys. Rev. D 41 (1990) 2675; ALEPH Coll., D. Buskulic et al.: Z. Phys. C 55 (1992) 209; DELPHI Coll., D. Aarnio et al.: Phys. Lett. B 240 (1990) 271; L3 Coll., B. Adeva et al.: Z. Phys. C 55 (1992) 39
42. S. Catani, L. Trentadue, G. Turnock, B.R. Webber: Nucl. Phys. B 407 (1993) 3
43. G. Dissertori, M. Schmelling: Phys. Lett. B 361 (1995) 167
44. Yu.L. Dokshitzer, A. Lucenti, G. Marchesini, G.P. Salam: JHEP 9801:011 (1998)
45. S. Catani, B.R. Webber: Phys. Lett. B 427 (1998) 377
46. S. Bethke: Nucl. Phys. B (Proc. Suppl.) 64 (1998) 54; S. Bethke: 'Jet Physics at LEP and the world summary of α_s', hep-ex/9812026
47. OPAL Coll., P. D. Acton et al.: Z. Phys. C 53 (1992) 539
48. OPAL Coll., R. Akers et al.: Z. Phys. C 68 (1995) 203
49. B.R. Webber: Phys. Lett. B 143 (1984) 501
50. JADE Coll., W. Bartel et al.: Z. Phys. C 20 (1983) 187; TASSO Coll., W. Braunschweig et al.: Z. Phys. C 45 (1989) 193; TPC Coll., H. Aihara et al.: Phys. Lett. B 134 (1987) 299; HRS Coll., M. Derrick et al.: Phys. Rev. D 34 (1986) 3304; AMY Coll., H. Zheng et al.: Phys. Rev. D 42 (1990) 737; MARK II Coll., G. Abrams et al.: Phys. Rev. Lett. 64 (1990) 1334; ALEPH Coll., D. Buskulic et al.: Z. Phys. C 69 (1995) 15; DELPHI Coll., P. Abreu et al.: Z. Phys. C 50 (1991) 185; L3 Coll., B. Adeva et al.: Z. Phys. C 55 (1992) 39; OPAL Coll., R. Akers et al.: Z. Phys. C 68 (1995) 203
51. Ya.I. Azimov et al.: Z. Phys. C 27 (1985) 65; Ya.I. Azimov et al.: Z. Phys. C 31 (1986) 213
52. Yu.L. Dokshitzer, V.S. Fadin, V.A. Khoze: Phys. Lett. B 115 (1982) 242; Yu.L. Dokshitzer, V.S. Fadin, V.A. Khoze: Z. Phys. C 15 (1982) 325
53. C.P. Fong, B.R. Webber: Nucl. Phys. B 355 (1991) 54
54. OPAL Coll., M.Z. Akrawy et al.: Phys. Lett. B 247 (1990) 617
55. TASSO Coll., W. Braunschweig et al.: Z. Phys. C 47 (1990) 187; MARK II Coll., A. Petersen et al.: Phys. Rev. D 37 (1988) 1; TPC Coll., H. Aihara et al.: LBL-23727 (1988); AMY Coll., Y. Li et al.: Phys. Rev. D 411 (1990) 2675; ALEPH Coll., D. Buskulic et al.: Z. Phys. C 55 (1992) 209; DELPHI Coll., P. Abreu et al.: Phys. Lett. B 275 (1992) 231; L3 Coll., B. Adeva et al.: Phys. Lett. B 229 (1991) 199
56. V.A. Khoze, S. Lupia, W. Ochs: B 386 (1996) 451
57. Yu.L. Dokshitzer, V.A. Khoze, S.I. Troyan: Int. J. Mod. Phys. A 7 (1992) 1875 V.A. Khoze, W. Ochs: J. of Mod. Phys. A 12 (1997) 2949
58. Yu.L. Dokshitzer, V.A. Khoze, S.I. Troyan: Z. Phys. C 55 (1992) 107
59. Yu.L. Dokshitzer, V.A. Khoze, S.I. Troyan: J. Phys. G 17 (1991) 1481
60. S. Lupia, W. Ochs: Phys. Lett. B 365 (1996) 339